A Simulator Comparison Study into the Effects of Motion Filter Order on Pilot Control Behavior

Pieters, Marc; Zaal, Peter; Pool, Daan; Stroosma, Olaf; Mulder, Max

DOI
10.2514/6.2019-0712

Publication date
2019

Document Version
Accepted author manuscript

Published in
AIAA Scitech 2019 Forum

A Simulator Comparison Study into the Effects of Motion Filter Order on Pilot Control Behavior

Marc A. Pieters*
San Jose State University
NASA Ames Research Center
Moffett Field, CA, USA
and
Delft University of Technology
Delft, the Netherlands

Peter M. T. Zaal †
San Jose State University
NASA Ames Research Center
Moffett Field, CA, USA

Daan M. Pool‡, Olaf Stroosma§, and Max Mulder¶
Delft University of Technology
Delft, the Netherlands

This paper describes an experiment investigating the effects of motion filter order on human manual control tracking behavior and performance. The experiment was performed on two simulators: the Vertical Motion Simulator at NASA Ames Research Center and the SIMONA Research Simulator at Delft University of Technology. Eighteen pilots in the Vertical Motion Simulator and twenty pilots in the SIMONA Research Simulator performed the experiment with a full factorial variation of three motion filter orders and two motion filter frequencies, in addition to a reference no-motion and full-motion condition. Motion shaping filters derived from Objective Motion Cueing Test measurements on the Vertical Motion Simulator were included in the SIMONA Research Simulator motion logic to match the motion cues between both simulators. Furthermore, the side sticks were set to matching characteristics and the visual cues were matched in terms of time delay, graphics size and screen characteristics. With increased motion filter order, pilots showed worse performance and a lowered contribution of motion feedback in their control strategy. Increasing the motion filter break frequency had similar effects, which were stronger than the effects of increasing the motion filter order, for the eight experimental conditions that were considered in this experiment. For the same motion condition the simulators showed offsets in the results. However, the trends between the motion conditions were similar, leading to the conclusion that for simulator comparisons relative trends are easier to replicate between simulators than absolute results within one condition.

*Research Scholar, Human Systems Integration Division, NASA Ames Research Center, Moffett Field, CA, 94035, and MSc. Student at the Control and Simulation Division, Faculty of Aerospace Engineering, Delft University of Technology, Delft, Netherlands; m.a.pieters@student.tudelft.nl. Student Member AIAA.

†Senior Research Engineer, Human Systems Integration Division, NASA Ames Research Center, Moffett Field, CA, 94035; peter.m.t.zaal@nasa.gov. Senior Member AIAA.

‡Assistant Professor, Control and Simulation Division, Faculty of Aerospace Engineering, P.O. Box 5058, 2600GB Delft, The Netherlands; d.m.pool@tudelft.nl. Member AIAA.

§Researcher, Control and Simulation Division, Faculty of Aerospace Engineering, P.O. Box 5058, 2600 GB Delft, The Netherlands; O.Stroosma@tudelft.nl. Senior Member AIAA.

¶Professor, Control and Simulation Division, Faculty of Aerospace Engineering, P.O. Box 5058, 2600 GB Delft, The Netherlands; M.Mulder@tudelft.nl. Senior Member AIAA.

Nomenclature

Symbols

e	error signal, deg
$f_{t,d}$	target / disturbance forcing function, deg
H_c	controlled dynamics
H_{mf}	motion filter
H_{motion}	motion hardware dynamics
$H_{shaping}$	motion shaping filter
H_{stick}	stick dynamics
H_{SRS}	SRS motion dynamics
$H_{p_{mot}}$	pilot motion response
$H_{p_{vis}}$	pilot visual response
H_{VMS}	VMS motion dynamics
K_m	motion gain, $-$
K_S	gain of motion filter at 1 rad/s, $-$
K_v	visual gain, $-$
n	pilot remnant, deg
O_{mf}	motion filter order, -
s	Laplace operator, $-$
t	time, s
T_L	pilot lead time constant, s
T_m	measurement time, s
u	pilot control input, deg
δ_c	control deflection, deg
ζ_{nm}	neuromuscular damping, $-$
θ	pitch angle, deg
μ	average, $-$
ρ	correlation coefficient, $-$
σ	standard deviation, $-$
σ_u^2	variance of control signal, deg^2
τ_m	motion time delay, s
τ_v	visual time delay, s
φ_m	open-loop phase margin, deg
Φ_S	phase of motion filter at 1 rad/s, deg
ω_c	open-loop crossover frequency, rad/s
ω_n	stick natural frequency, rad/s
ω_{mf}	motion filter frequency, rad/s
ω_{nm}	neuromuscular frequency, rad/s
ω_{phug}	phugoid frequency, rad/s
ω_{sp}	short period frequency, rad/s

Abbreviations

ANOVA	analysis of variance
CG	center of gravity
ERP	eye reference point
ICR	instantaneous center of rotation
IDMS	Image Delay Measurement System
KW	Kruskall-Wallis test
MLE	maximum likelihood estimation
OMCT	Objective Motion Cueing Test
PFD	primary flight display
REF	reference motion conditions
RMS	root mean square
SRH	Scheirer-Ray-Hare extension
SRS	SIMONA Research Simulator
T-CAB	transport aircraft cab
VAF	variance accounted for
VDMS	Visual Delay Measurement System
VMS	Vertical Motion Simulator

I. Introduction

This paper presents the results of an experiment that was performed on two simulators investigating changes in pilot control behavior and performance for different motion filter orders.

The aviation market is growing and over the next 20 years it is estimated that over 600,000 new pilots are required.[1,2] With such a predicted increase, industry is eager to train pilot control skills efficiently. Traditionally, in order to train pilots efficiently, flight simulators are designed to present pilots with high fidelity simulation cues,[3] such as motion cues. However, even though the benefit of using motion-enabled flight simulators in the training of pilot control skills is the subject of much debate,[4–7] current pilot training requirements still focus heavily on the availability of motion in flight simulators. The focus on motion is even growing, which is illustrated by the new requirement for airline pilots to receive stall training in full-motion flight simulators starting in 2019.[8–10] Hence, with the increasing need for skilled pilots in the growing aviation industry, the role of motion in flight simulators will become more important.

Flight simulators are bound by their available motion space in presenting pilots with motion cues. A large variety of motion washout filters has been applied in the past, in order to make pilots perceive the onset of a maneuver without exceeding the physical limits of the motion system.[11] Classical washout filters are commonly used since they ensure different pilots are presented with the same motion cues, independent of their control behavior.[12] The settings of classical washout filters have been shown to influence pilot control behavior in numerous studies.[13–21] Hence, the effects of the motion filter settings on pilot control behavior and performance need to be known, in order to determine how pilots could benefit from motion in flight simulators.

Whereas the parameters of the classical washout filters (gains, break frequencies, rate limits, etc.) have been the

subject of numerous studies,[7,13,14,22–24] the order of the washout filters O_{mf} has not received the same attention. For example, Pool et al.[13,14] consolidated the results of ten studies into the effects of motion fidelity on pilot control behavior using quantitative cybernetic pilot models. They found consistent results indicating that a decreasing motion filter gain K_{mf} and an increasing motion filter break frequency ω_{mf}, result in degraded pilot performance, lower visual gains and increased use of visual information for lead generation. Furthermore, the parameters have been the subject of studies in which procedures for tuning the washout filters were investigated.[7,22–24]

Furthermore, despite the need for verification of human performance results, experiments on full-motion flight simulators are rarely replicated due to high costs involved and challenges in comparing simulator subsystems. In a series of previous flight simulation experiment replications where a yaw-capture task with varying sway and yaw cueing was considered, generally similar results were found.[25–31] However, differences between the simulators were present even though considerable effort was spent on matching all experiment setups. Another replication by Jex et al.[32,33] considered a tracking task, which proved valuable in comparing the control behavior of pilots between simulators, and identifying the source of the possible differences. Hence, repeating a manual control tracking experiment on two simulators while matching simulation cues, would allow for verification of current findings of filter order effects and might aid in drawing conclusions for future simulator comparisons.

This paper has two main goals. The first goal is to gain insight into the effects of motion filter order O_{mf} and motion filter break frequency ω_{mf} on pilot manual control behavior and performance. This was achieved by performing an experiment with a variation of the order of the motion filters. A pitch task based on Ref. 34 was performed, which allowed the use of cybernetic pilot models to assess changes in control behavior and performance in a quantitative manner. In total, 38 pilots participated in the experiment. The second goal of this paper is to determine factors for generalizability of experimental findings into human control behavior and performance on multiple simulators, in order to aid future experiment replications. This was done by performing the experiment on both the Vertical Motion Simulator (VMS) and the SIMONA Research Simulator (SRS) and comparing the results. Because of the dual goal of the paper, two sets of hypotheses are present: the first three hypotheses discuss the motion filter effects and two hypotheses are added to cover the simulator comparison aspect.

Section II presents the methodology of the experiment. Then, Section III elaborates on the efforts to match the cues the pilots perceived in both simulators. Section IV presents the experimental results. In Section V, the results are discussed. Finally, Section VI concludes the paper.

II. Method

II.A. Control Task

The manual pitch control task that participants performed in both the VMS and SRS can be represented by the closed-loop diagram in Figure 1. The task was based on a previous experiment by Zaal and Zavala.[34] Comparing the results of Ref. 34 to the current experimental results allowed to verify correct implementation of the task on both simulators. Furthermore, using an existing task minimized development time on the two flight simulators. Participants were asked to minimize the pitch error e, which was presented on a compensatory display, by making inputs with a side stick. The display represented a simplified version of a primary flight display (PFD). Using the side stick pilots generated control inputs u. The inputs acted on the pitch dynamics transfer function $H_\theta(s)$, which resulted in the pitch angle θ. This pitch angle θ was used to calculate the visual pitch error signal e. Furthermore, in the motion feedback path, it was filtered through a motion filter $H_{mf}(s)$. The motion filter $H_{mf}(s)$ was applied to all symmetric motion channels and varied between experimental conditions (see Section II.E). The pilot perceived the motion cues resulting from the motion system $H_{motion}(s)$. In the VMS the motion system just consisted of the VMS motion system dynamics $H_{motion_{VMS}}(s)$. In the SRS a motion shaping filter $H_{shaping}(s)$ was present in front of the SRS motion system dynamics: $H_{motion}(s) = H_{shaping}(s) \cdot H_{motion_{SRS}}(s)$, in order to match the motion system response of the SRS to the VMS (see Section III.A). Finally, two forcing functions were present which allowed to identify a multi-channel quasi-linear human pilot model which consisted of a visual response function $H_{p_{vis}}(s)$, a motion response function $H_{p_{mot}}(s)$ and a remnant signal n.[35] The remainder of this section goes more into depth on the individual elements of Figure 1.

II.A.1. Controlled Dynamics

The controlled dynamics $H_\theta(s)$ were defined by Eq. (1). They represent a mid-size twin-engine commercial transport aircraft with a weight of 185,000 lbs, trimmed close to its stall point at 41,000 ft and with an indicated airspeed of 150 kts. The controlled dynamics feature a stable short period eigenmode ($\omega_{sp} = 0.6892$ rad/s) and an unstable phugoid eigenmode ($\omega_{phug} = 0.0638$ rad/s), with eigenvalues at $\lambda_{1,2} = -0.2230 \pm 0.6522i$ and $\lambda_{3,4} = 0.0069 \pm 0.0634i$ in

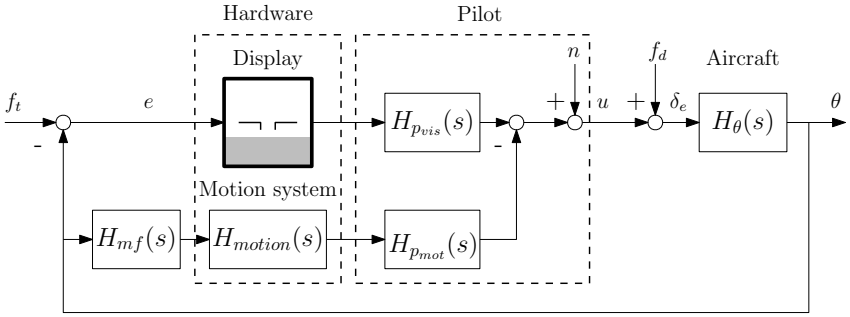

Figure 1: The considered pitch control task and human pilot model

the complex plane, respectively. These controlled dynamics were used earlier in Ref. 34.

$$H_\theta(s) = \frac{\theta(s)}{\delta_e(s)} = \frac{28.4474 \cdot \left(346.5s^2 + 32.03s + 1\right)}{(245.6s^2 - 3.409s + 1) \cdot (2.105s^2 + 0.9387s + 1)} \tag{1}$$

Vertical motion of the center of gravity (CG) of the aircraft results in CG heave. Instantaneous center of rotation (ICR) pitch-heave results from the location of the pilot station in front of the center of rotation. The pilot of a real aircraft feels a combination of both heave components. To accommodate the motion space of both simulators, no CG heave was present and only ICR pitch-heave was included in the task. A previous study showed that this did not significantly affect pilot control behavior.[36] The ICR pitch-heave response to pitch variations was defined by Eq. (2).

$$H_{a_{z_{\theta,ICR}}}(s) = \frac{a_{z_{\theta,ICR}}(s)}{\theta(s)} = -11.49s^2 \tag{2}$$

Eq. (2) shows that the pilot station was located 11.49 m in front of the instantaneous center of rotation. Analogous to ICR pitch heave, the z-position of the pilot station above or below the x-axis of the aircraft body-fixed reference frame results in ICR pitch surge. In the considered aircraft, the pilot station was placed on the x-axis, such that no pitch surge was present. Furthermore, no CG surge was modelled.

II.A.2. Human Pilot Model

In order to investigate the control behavior of the pilot, linear transfer functions were identified for both the visual and the motion channel, as depicted in Figure 1. McRuer and Jex[37] state that pilots adapt themselves to the controlled dynamics to ensure that the open-loop response approximates a single integrator in the region of the crossover frequency. For the controlled dynamics of Eq. (1), pilots thus need to generate lead in the region of the crossover frequency. Hence, the pilot visual and motion responses are defined by Eq. (3) and (4), respectively.

$$H_{p_{vis}}(s) = K_v \left(1 + T_L s\right) e^{-\tau_v s} \frac{\omega_{nm}^2}{s^2 + 2\zeta_{nm}\omega_{nm}s + \omega_{nm}^2} \tag{3}$$

$$H_{p_{mot}}(s) = sK_m e^{-\tau_m s} \frac{\omega_{nm}^2}{s^2 + 2\zeta_{nm}\omega_{nm}s + \omega_{nm}^2} \tag{4}$$

These two equations formed the pilot model, which has a total of seven parameters that quantify pilots' selected control behavior. The pilot lead equalization is captured with the equalization parameters: the visual gain K_v, the motion gain K_m, and the lead time constant T_L. The human limitations of the pilots are captured with the visual time delay τ_v and the motion time delay τ_m. Furthermore, pilots are limited by their neuromuscular actuation, which is captured with the neuromuscular parameters: the damping constant ζ_{nm} and frequency ω_{nm}. Previous research has shown that a second-order mass-spring-damping model is able to adequately describe the combined stick and neuromuscular dynamics of the pilots.[15,36,38]

II.A.3. Forcing Functions

Two forcing functions were used in the pitch tracking task, a target and a disturbance signal, which resulted in a combined target-following and disturbance-rejection task. Using two independent forcing function signals allowed to estimate the two separate describing functions that are part of the pilot model as introduced in Section II.A.2: the pilot

visual response $H_{p_{vis}}$ and the pilot motion response $H_{p_{mot}}$.[14] Both forcing functions were defined as sum-of-sines signals:

$$f_{t,d}(t) = \sum_{k=1}^{N_{t,d}} A_{t,d}(k) \sin\left[\omega_{t,d}(k)t + \phi_{t,d}(k)\right] \tag{5}$$

In Eq. (5) $A_{t,d}(k)$, $\omega_{t,d}(k)$ and $\phi_{t,d}(k)$ represent the amplitude, frequency and phase of the k^{th} sine in the target and disturbance forcing functions f_t and f_d, respectively. The number of sine waves in these functions is represented by $N_{t,d}$. The considered forcing function parameter values for the f_t and f_d signals, both with $N_{t,d} = 10$ sinusoids, can be found in Table 1.

Table 1: Properties of the forcing functions, as found in Ref. 34

Target, f_t				Disturbance, f_d			
n_t [-]	ω_t [rad/s]	A_t [deg]	ϕ_t [rad]	n_d [-]	ω_d [rad/s]	A_d [deg]	ϕ_d [rad]
3	0.2301	0.5818	-1.4796	2	0.1534	0.0105	0.1355
6	0.4602	0.5306	-0.0745	5	0.3835	0.0098	-0.1664
13	0.9971	0.3711	0.7006	11	0.8437	0.0091	2.9016
27	2.0709	0.1674	-1.9563	23	1.7641	0.0283	5.6383
41	3.1447	0.0901	-2.8131	37	2.8379	0.0403	2.8648
53	4.0650	0.0605	2.1026	51	3.9117	0.0477	4.8718
73	5.5990	0.0375	-2.6178	71	5.4456	0.0569	1.0245
103	7.9000	0.0238	2.2550	101	7.7466	0.0725	5.0337
139	10.6612	0.0174	-0.6739	137	10.5078	0.0967	4.1487
194	14.8796	0.0135	0.1942	191	14.6495	0.1458	0.4274

The frequencies for the sinusoids ($\omega_{t,d}$) were all integer multiples ($n_{t,d}$) of the measurement time base frequency, $\omega_m = 2\pi/T_m = 2\pi/81.92$ s $= 0.0767$ rad/s, to avoid spectral leakage. The integer multiples were selected to ensure that the typical frequency range of human control was covered with regular intervals on a logarithmic scale.[34] Both the target forcing function f_t and the disturbance forcing function f_d had a time-domain variance of 0.4 deg^2, which has been applied successfully in previous experiments.[34]

The runs lasted 94.92 seconds. The first 3 seconds contained no forcing functions, followed by 5 seconds of ramp-in, to allow pilots to stabilize the controlled element. Then, a measurement window of 81.92 seconds was used for the analysis. The last 5 seconds were a fade-out of the forcing functions, in order to return the simulators to their initial positions gradually.

II.B. Dependent Measures

The goal of the experiment was to investigate how the order of the motion washout filter O_{mf} and the motion filter frequency ω_{mf} influenced the control behavior of the pilots and whether results were comparable between two flight simulators. Hence, human control behavior and performance parameters were the variables of interest.

The root mean square (RMS) of the error signal e (i.e. RMS_e) and control signal u (i.e. RMS_u) were determined. RMS_e is a measure of performance, where a lower RMS_e signifies a lower overall error score and hence a better performance. RMS_u is a measure of control activity; a higher RMS_u indicates a higher control activity.

Furthermore, the pilot model defined in Eqs. (3) and (4) featured seven dependent variables: K_v, K_m, T_L, τ_v, τ_m, ζ_{nm} and ω_{nm}. These parameters were estimated using a time-domain parameter estimation technique, based on maximum likelihood estimation (MLE).[36] In this technique, a genetic algorithm provides an initial estimate for the parameters, which is subsequently refined by a gradient based Gauss-Newton estimation. The variance accounted for (VAF) is a measure of how much of the control signal u could be explained by the linear pilot model transfer functions. Using the linear pilot model transfer functions, the variance of the control signals of both the visual and motion channel, $\sigma^2_{u_v}$ and $\sigma^2_{u_m}$, respectively, were computed. The fraction of these variances showed how much of the total control signal u could be explained by the two channels of the quasi-linear pilot model.

Finally, the crossover frequencies and phase margins of the open-loop dynamics describe the pilot performance in attenuating the target and disturbance signals.[34] Looking at Figure 1, an open-loop response can be constructed, for both the target and disturbance inputs, which can be seen in Eq. (6) and (7), respectively.

$$H_{ol,t}(s) = \frac{\theta(s)}{E(s)} = \frac{H_{p_{vis}}(s)H_\theta(s)}{1 + H_{mf}(s)H_{motion}(s)H_{p_{mot}}(s)H_\theta(s)} \tag{6}$$

$$H_{ol,d}(s) = -\frac{U(s)}{\delta_c(s)} = H_\theta(s)\left[H_{p_{vis}}(s) + H_{mf}(s)H_{motion}(s)H_{p_{mot}}(s)\right] \tag{7}$$

The open-loop crossover frequencies and phase margins for both the target and disturbance signal were determined, using Eqs. (6) and (7): $\omega_{c,t}$, $\omega_{c,d}$, $\varphi_{m,t}$ and $\varphi_{m,d}$.

II.C. Participants

In the VMS 18 pilots participated in the experiment and in the SRS 20 pilots participated. All participants were active general aviation pilots. Table 2 presents information on the pilot population. Four VMS pilots had considerably more flight hours than the rest: 5300, 2800, 1637 and 1200 hours. Similarly, two SRS pilots had flown considerably more hours than the rest: 6800 and 1018 hours. Most pilots in both groups had experience in fixed-base or full-motion flight simulators. Most of the VMS pilots had experience with similar experiments (for example, Ref. 37), whereas the recruited SRS pilots did not.

Data from one VMS pilot and one SRS pilot were removed. For the VMS pilot the data were not sufficient to generate accurate parameter estimates and the SRS pilot was not able to complete the experiment. Consequently, the analysis of the results was performed with another two random SRS pilots omitted, such that for both simulators the data of 17 pilots were present, as one of the statistical tests assumed an equal number of participants in both groups, as explained in Section IV.A.

Table 2: Overview of pilot population characteristics

	Age		Flight hours		Simulator hours		Flight and simulator hours past 3 months	
	μ	σ	μ	σ	μ	σ	μ	σ
VMS	28.9	4.97	751	1341	45.7	91.0	17.3	40.3
SRS	31.5	5.52	636	1445	27.9	60.2	37.3	58.4

II.D. Procedures

At the start of the experiment, each pilot was given a briefing, detailing the purpose of the experiment and the procedures, including suggestions and examples on how to best follow the target and compensate for the disturbance. No specifics about the (number of) motion conditions were given, except that a no-motion condition was present. Pilots were informed of the current best score and encouraged to improve it. After each run the head down display showed the RMS_e of that run to give the pilots feedback on their performance.

The experiment consisted of three simulator sessions, all performed on the same day, with breaks in between sessions. The pilots performed 24, 20 and 12 runs in the first, second and third session, respectively. During and between each session pilots were informed that they could take additional or longer breaks if they so desired (for example, due to fatigue). The first 16 runs were used as training and the last 40 runs were used to calculate the results. A randomized latin square experiment matrix was followed. Over the full experiment, each pilot performed each experimental condition 7 times.

Brown noise resembling aircraft engines was played over noise-cancelling headphones to mask the sound made by the motion actuators throughout the experiment.

II.E. Independent Variables

Table 3 shows the eight tested experimental conditions. The motion filters in these conditions were applied to the pitch, heave and surge axes of the simulators. Three motion filter orders and two break frequencies were tested. C0 and C7 are reference (REF) motion conditions. C0 is a reference no-motion condition and C7 acts as a reference full-motion condition. The no-motion condition C0 was present to isolate the effects of the motion system of the simulators. For C0 the pilot model only consisted of a visual channel. The full-motion condition C7 was implemented as a second order filter with a break frequency of $\omega_{mf} = 0.2$ rad/s, in order to prevent the simulator from drifting. It was present to generate the motion shaping filters $H_{shaping}(s)$ (see Section III) and as a reference motion value for the prediction

equations. In all conditions, the damping constant was set to $\zeta_{mf} = 1/\sqrt{2} = 0.707$. Figure 2 shows the fidelity of the motion conditions against the fidelity criteria proposed by Sinacori[39] and Schroeder.[25] With increasing filter order O_{mf}, the conditions move further away from the high fidelity region. This effect is present for increasing motion filter frequency ω_{mf} as well, with even bigger changes visible.

Table 3: Experimental conditions

Condition	Filter order O_{mf} [-]	ω_{mf} [rad/s]	Motion Filter	K_S [-]
C0	No motion	-	$H_{mf}(s) = 0$	0.000
C1	1	0.5	$H_{mf}(s) = \frac{s}{s+0.5}$	0.894
C2	1	2.0	$H_{mf}(s) = \frac{s}{s+2.0}$	0.447
C3	2	0.5	$H_{mf}(s) = \frac{s^2}{s^2+2\cdot\zeta_{mf}\cdot 0.5\cdot s+0.5^2}$	0.970
C4	2	2.0	$H_{mf}(s) = \frac{s^2}{s^2+2\cdot\zeta_{mf}\cdot 2.0\cdot s+2.0^2}$	0.243
C5	3	0.5	$H_{mf}(s) = \frac{s}{s+0.5}\cdot\frac{s^2}{s^2+2\cdot\zeta_{mf}\cdot 0.5\cdot s+0.5^2}$	0.868
C6	3	2.0	$H_{mf}(s) = \frac{s}{s+2.0}\cdot\frac{s^2}{s^2+2\cdot\zeta_{mf}\cdot 2.0\cdot s+2.0^2}$	0.109
C7	Full motion	0.2	$H_{mf}(s) = \frac{s^2}{s^2+2\cdot\zeta_{mf}\cdot 0.2\cdot s+0.2^2}$	0.999

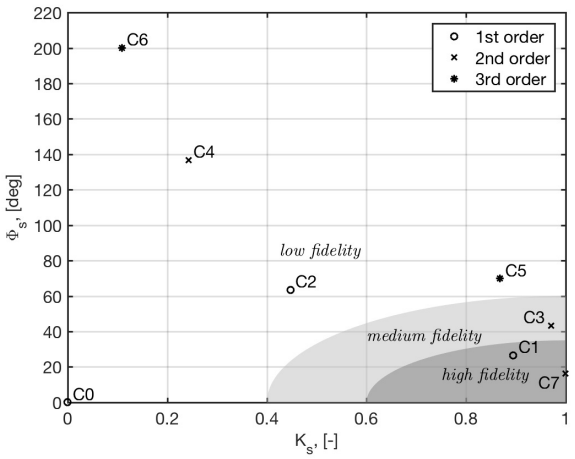

Figure 2: Experiment conditions shown on motion fidelity plot, as proposed by Ref. 39 and Ref. 25

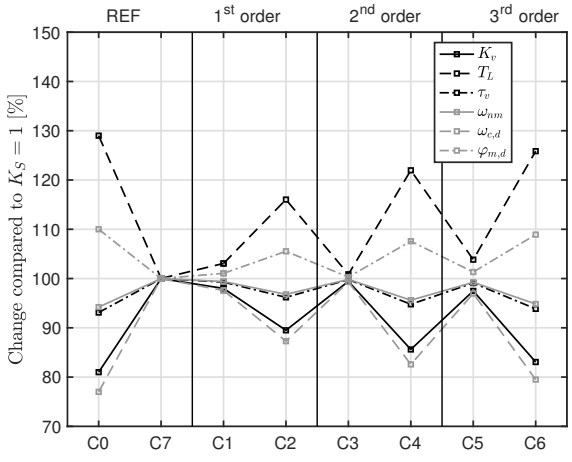

Figure 3: Predicted relative change of pilot model parameters, in comparison to full-motion C7

II.F. Hypotheses

Pool et al. formulated a series of equations in Ref. 13 that predict the effects of different motion filter settings on the dependent variables mentioned before. Using these equations, the effects of changing O_{mf} and ω_{mf} could be predicted. By analyzing data from numerous studies where motion conditions were varied and the effects on pilot tracking and control behavior were investigated, it was found that K_S, the magnitude of the motion filter at a frequency of 1 rad/s, was the most suitable predictor variable.[13] K_S is part of the motion fidelity criteria as proposed by Sinacori[39] and adapted by Schroeder.[25] It was calculated using Eq. (8).

$$K_S = |H_{mf}(j\omega)|_{\omega=1\ rad/s} \tag{8}$$

The prediction equations relate the pilot model parameters to the motion fidelity of a certain motion condition, using K_S. Using the value of a reference full-motion condition with $K_S = 1$, the K_S of the desired condition allows to compute the corresponding predicted pilot model parameter. The prediction equations are given by Eq. (9) to (14).

$$\hat{K}_v(K_S) = K_v(1)\left[0.19\left(K_S - 1\right) + 1\right] \tag{9}$$

$$\hat{T}_L\left(K_S\right) = T_L(1)\left[-0.29\left(K_S - 1\right) + 1\right] \tag{10}$$

$$\hat{\tau}_v\left(K_S\right) = \tau_v(1)\left[0.069\left(K_S - 1\right) + 1\right] \tag{11}$$

$$\hat{\omega}_{nm}\left(K_S\right) = \omega_{nm}(1)\left[0.058\left(K_S - 1\right) + 1\right] \tag{12}$$

$$\hat{\omega}_{c,d}(K_S) = \omega_{c,d}(1)\left[0.23\left(K_S - 1\right) + 1\right] \tag{13}$$

$$\hat{\varphi}_{m,d}(K_S) = \varphi_{m,d}(1)\left[-0.10\left(K_S - 1\right) + 1\right] \tag{14}$$

For example, for $\hat{T}_L$, the prediction of the lead time constant T_L, the value of the lead time constant in a condition with $K_S = 1$ is indicated by $T_L(1)$ and K_S is the value of the motion condition of the desired prediction. The numerical factor that follows (-0.29 in the case of $\hat{T}_L$) indicates the percentage change that occurs when K_S equals 0: the lead time constant is predicted to be 29% higher for $K_S = 0$ than for $K_S = 1$.[13] Pool et al.[13] found sufficiently strong linear regressions between K_S and the following pilot model parameters: K_v, T_L, τ_v, ω_{nm}, $\omega_{c,d}$ and $\varphi_{m,d}$. For K_m, τ_m, ζ_{nm}, $\omega_{c,t}$ and $\varphi_{m,t}$ no such linear relationships were found.

Figure 3 shows the predicted relative change for each experimental motion condition compared to C7, with $K_S = 1$ in percent. Because C7 was implemented as a second order filter with $\omega_{mf} = 0.2$ rad/s, its K_S was equal to 0.999, see Table 3. For increasing motion filter order O_{mf}, increases in T_L and $\varphi_{m,d}$ can be seen. Furthermore, K_v and $\omega_{c,d}$ show a decrease for increasing filter order. τ_v and ω_{nm} show slight decreases for increasing O_{mf} as well. The effects are similar, but more pronounced for increasing motion filter break frequency ω_{mf}. For the increasing filter order O_{mf}, mainly the $\omega_{mf} = 2.0$ rad/s conditions show the changes.

Based on the offline prediction equations, three hypotheses were formulated for the change in dependent measures due to the change in filter order O_{mf} and filter frequency ω_{mf}, respectively:

H1: **Effect of motion filter order** O_{mf} - With increasing motion filter order more of the low frequency content of the aircraft output is filtered out by the motion filter. Furthermore, a higher filter order leads to more induced phase lead on the simulator motion. In Figure 3 it can be seen that for an increase in motion filter order the prediction equations predicted a decrease in visual gain K_v, an increase in visual lead time constant T_L and a slight decrease in visual time delay τ_v and neuromuscular frequency ω_{nm}. Mainly for the higher motion filter break frequency $\omega_{mf} = 2.0$ rad/s the effects for increasing the motion filter order are visible. Thus, it was expected that pilots would control with a smaller gain, while using more of the visual channel to generate lead. Furthermore, the prediction equations predicted a decrease in disturbance crossover frequency and a corresponding increase in disturbance phase margin. This suggested that the pilot model motion channel $H_{p_{mot}}$ would contribute less to the open-loop responses. Hence, it was hypothesized that pilots would use less motion and their performance would decrease for increasing motion filter order.

H2: **Effect of motion filter frequency** ω_{mf} - Similar to H1, with increasing motion filter break frequency ω_{mf}, more of the low-frequency content of the aircraft output is filtered out by the motion filter. Figure 2 relates this to a lowered motion fidelity. Looking at Figure 3 it can be seen that most of the effects are similar to the ones stated in hypothesis H1, albeit stronger. It was expected that with an increase in motion filter break frequency ω_{mf}, pilots would display an increase in T_L and $\varphi_{m,d}$ and a decrease K_v and $\omega_{c,d}$ and a slight decrease in τ_v and ω_{nm}. Thus, it was hypothesized that pilots would also use less motion and their performance would decrease for increasing motion filter frequency ω_{mf}.

H3: **Motion filter order versus motion filter frequency** - When comparing the different motion filter break frequencies to the motion filter orders in Figure 2 and 3, the change in frequency ω_{mf} showed larger changes in K_S. Subsequently, the prediction equations predicted larger changes on the pilot model parameters for changing ω_{mf} than for changing O_{mf}. Therefore, the effects of O_{mf} were hypothesized to be less severe than the effects of ω_{mf}, for the considered experimental conditions.

Hypotheses H1, H2 and H3 treat the effects of the independent variables O_{mf} and ω_{mf}. They will be supplemented with another two hypotheses in Section III that focus on the use of two different simulators.

III. Simulator Equalization

The experiment was first performed on the VMS at NASA Ames Research Center, using the transport aircraft cab (T-CAB), see Figure 4. The SRS at Delft University of Technology was used to replicate the experiment, see Figure 5. Their respective cockpits are visible in Figures 6 and 7. Figures 8 and 9 present the dimensions of the cockpit and location of the control device, the head-down display and the eye reference point (ERP) of both simulators.

Figure 4: The VMS (Ref. 40)

Figure 5: The SRS (Ref. 41)

Figure 6: VMS cockpit (Ref. 42)

Figure 7: SRS cockpit (Ref. 15)

Figure 10 shows a high-level schematic overview of a pilot executing a task in a flight simulator.[43] The pilot receives cues from the task and several simulator systems involved in the simulation: the motion system, the visual system, the control device feedback, proprioceptive feedback and feedback from secondary cues. The following sections discuss the equalization of these systems and their cues across both simulators, according to the division in Figure 10.

III.A. Motion System

The VMS was built to provide the motion fidelity needed to simulate vertical take-off and landing vehicles and hence features a heave range of motion of $\pm$ 9.14 m. The cabin can also move $\pm$ 6.10 m laterally and $\pm$ 1.22 m longitudinally.[40] The vertical and lateral motion is provided by electric motors, while for the longitudinal and rotational motions hydraulic actuators are used. The 6 degrees-of-freedom are uncoupled. On the other hand, the SRS has a hydraulic hexapod motion system with linear actuators that have an operational stroke length of 1.15 m.[12]

Shaping filters were estimated to equalize the motion response between simulators for the pitch and heave axes. The shaping filters had the following form[29] and were placed between the aircraft output and the motion filters on the SRS, see Figure 1:

$$H_{shaping}(s) = H_{SRS}^{-1}(s) \cdot H_{VMS}(s) \tag{15}$$

where $H_{SRS}(s)$ and $H_{VMS}(s)$ represent the unaltered motion frequency responses of the SRS and VMS, respectively. Objective Motion Cueing Test (OMCT)[44] measurements were performed for the full-motion experimental condition C7 on both simulators prior to the experiment to determine the unaltered motion response at twelve discrete OMCT

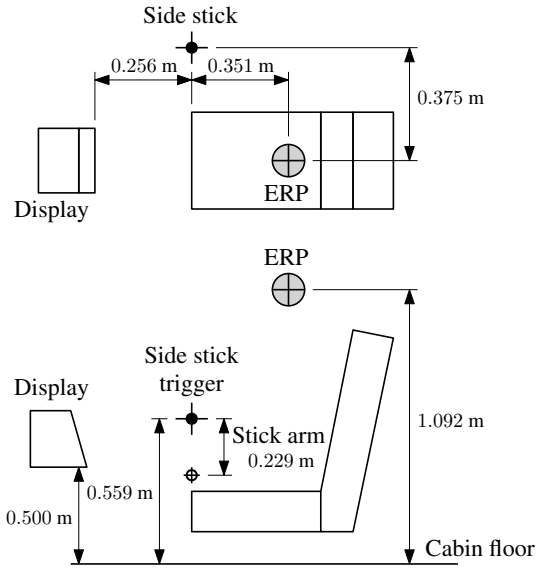

Figure 8: VMS cockpit dimensions, not to scale

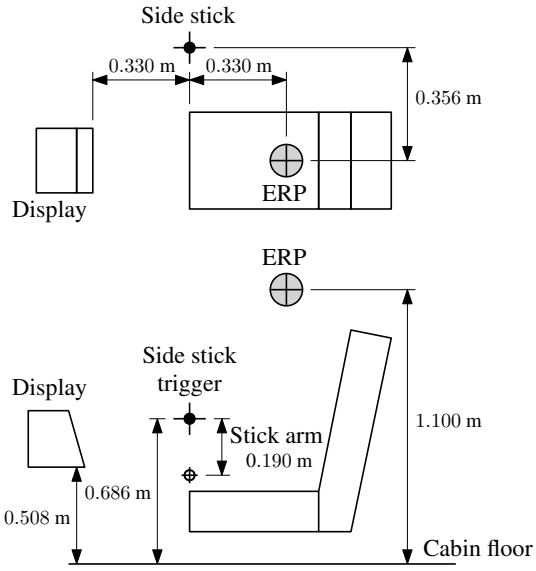

Figure 9: SRS cockpit dimensions, not to scale

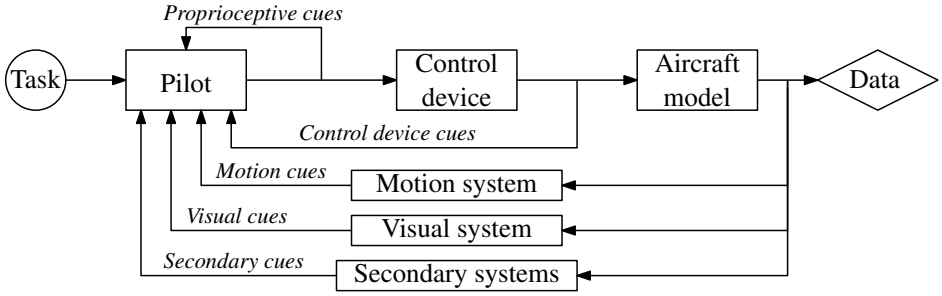

Figure 10: Schematic representation of a pilot executing a task in a flight simulator, as adapted from Ref. 43

measurement frequencies. Then, transfer functions of the form presented in Eq. (16) were fitted through the twelve OMCT response measurement points using a quadratic cost function,[29] to determine the simulator motion dynamics.

$$H_{SRS,VMS}(s) = \frac{A \cdot s^2}{B \cdot s^2 + C \cdot s + D} \cdot e^{-E \cdot s} \tag{16}$$

The resulting simulator motion dynamics for the relevant degrees of freedom of the VMS and SRS were as follows:

$$H_{VMS_z}(s) = \frac{0.911 \cdot s^2}{0.883 \cdot s^2 + 0.280 \cdot s + 0.036} \cdot e^{-0.098 \cdot s} \tag{17}$$

$$H_{VMS_q}(s) = \frac{0.893 \cdot s^2}{0.916 \cdot s^2 + 0.254 \cdot s + 0.035} \cdot e^{-0.045 \cdot s} \tag{18}$$

$$H_{SRS_z}(s) = \frac{0.908 \cdot s^2}{0.900 \cdot s^2 + 0.256 \cdot s + 0.036} \cdot e^{-0.045 \cdot s} \tag{19}$$

$$H_{SRS_q}(s) = \frac{0.908 \cdot s^2}{0.891 \cdot s^2 + 0.259 \cdot s + 0.035} \cdot e^{-0.026 \cdot s} \tag{20}$$

Because of limitations due to the chosen experimental motion conditions (Section II.E), the standard OMCT test signal amplitudes as specified in Ref. 44 did not fit in the available motion space: some of the lower frequencies exceeded limits in the SRS and some of the higher frequencies exceeded limits in the VMS. This was due to the motion filter gain being $K_{mf} = 1.0$ in all conditions. Hence, using simulations of the motion systems of both simulators,

the amplitudes were adapted according to Table 4. Two sets of OMCT tests were performed. Firstly, the full-motion simulator settings (experimental condition C7) were used to construct the shaping filters of Eqs. (17) to (20). Secondly, with the shaping filters present, the motion filter settings of experimental condition C5 were used as verification, as this experimental condition was the furthest away from the full-motion condition C7, in terms of motion filter order: it had a third order filter. Condition C5 had a break frequency of $\omega_{mf} = 0.5$ rad/s, which allowed to construct the motion frequency responses with a sufficiently high test signal-to-noise ratio. Due to its break frequency of $\omega_{mf} = 2.0$ rad/s, C6 could not be used for the verification OMCT data, as too much of the low frequency signals were found to be filtered away with the adapted amplitude settings.

Table 4: OMCT signal amplitudes

	Standard OMCT amplitudes		C7 OMCT amplitudes		C5 OMCT amplitudes	
Frequency	Linear [m/s^2]	Rotational [deg/s^2]	Linear [m/s^2]	Rotational [deg/s^2]	Linear [m/s^2]	Rotational [deg/s^2]
1	1.000	0.060	0.010	0.060	0.500	1.000
2	1.000	0.150	0.010	0.150	0.500	1.000
3	1.000	0.251	0.020	0.251	0.250	0.251
4	1.000	0.398	0.050	0.398	0.250	0.398
5	1.000	0.631	0.050	0.631	0.250	0.631
6	1.000	1.000	0.100	1.000	0.500	1.000
7	1.000	1.585	0.500	1.585	1.000	1.585
8	1.000	2.512	1.000	2.512	1.000	2.512
9	1.000	3.981	1.000	3.500	1.000	3.500
10	1.000	6.310	1.000	6.000	1.000	6.000
11	1.000	10.000	1.000	7.000	1.000	7.000
12	1.000	10.000	1.000	7.000	1.000	7.000

Figure 11 shows the unaltered motion responses of both simulators and the SRS response with the shaping filter included for C7. Figure 12 shows the same for experimental condition C5. In both figures it can be seen that the shaping filter succeeds in matching the SRS to the original unaltered VMS motion response for the heave degree-of-freedom. The pitch degree-of-freedom showed similar results, which are omitted here for the purpose of brevity.

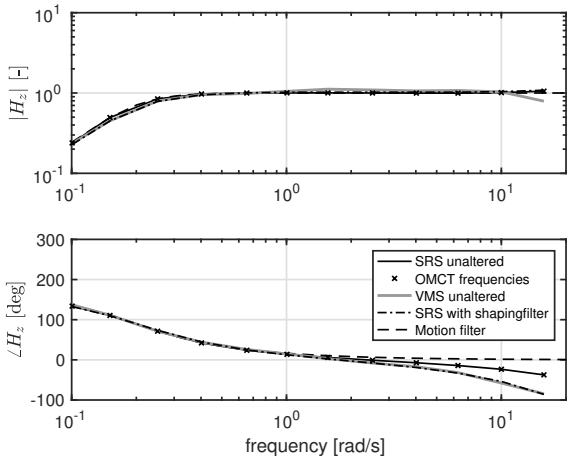

Figure 11: Motion response of the VMS compared to the SRS with and without shaping filter for the full-motion condition C7, that was used to construct the shaping filters

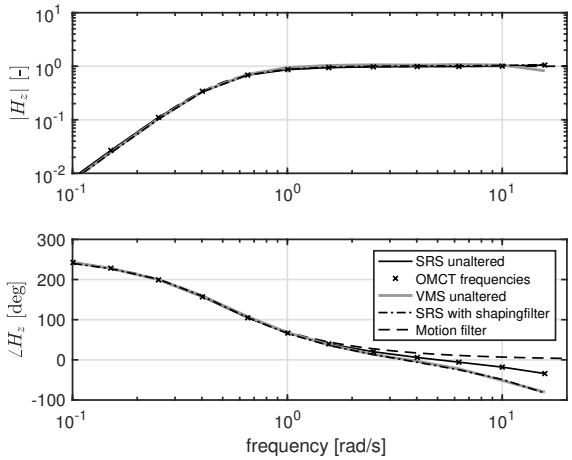

Figure 12: Motion response of the SRS with the shaping filters included and the unaltered response of the VMS for a third order motion filter (experimental condition C5)

III.B. Control Device

The VMS featured a electro-hydraulic McFadden control side stick,[45] whereas the SRS has an electrical Moog side stick. Both simulators featured an armrest. The armrest in the VMS was covered with a canvas fabric, which allowed the pilots' arm to slide relatively freely over the armrest. The armrest in the SRS was covered with artificial leather, which prevented free movement of the arm to a certain degree. Table 5 presents the parameters of the side stick used

in the experiment. In both simulators the side stick settings were set to these values, which were subsequently verified using a force-displacement plot on both simulators and a frequency sweep on the SRS. Figure 13 shows the force-displacement plot. The force-displacement allowed to verify that the gradient, the breakout and the range of motion of the side sticks was the same. Figure 14 shows a frequency sweep that was performed on the SRS. The natural frequency of the SRS stick was found by fitting a mass-spring-damper transfer function to the stick dynamics H_{stick} that were determined from the frequency sweep data. The stick dynamics H_{stick} were determined as follows:

$$H_{stick}(s) = \frac{U(s)}{F(s)} \tag{21}$$

where $U(s)$ and $F(s)$ are the Fourier-transformed control signal (i.e. stick position) and stick stick force, respectively. The natural frequency of the VMS side stick was found to be $\omega_n = 11.04$ rad/s by manually adjusting a mechanical damping factor in the side stick hardware and subsequently letting the stick oscillate in its natural frequency after a small perturbation. Figure 14 shows that the mass-spring-damper transfer function that was fitted on the SRS frequency sweep data crosses the -90 degrees phase line at $\omega_n = 11.08$ rad/s. One difference between the two side sticks that could not be adjusted was the length of the stick arm, which was 0.229 m in the VMS and 0.190 m in the SRS, as measured from the turning point to the trigger, as can be seen in Figure 8 and 9. Furthermore, the design of the grip of both sticks was different. The position of the side sticks with respect to the seat differed 0.02 m. No adjustments were made to correct for this offset.

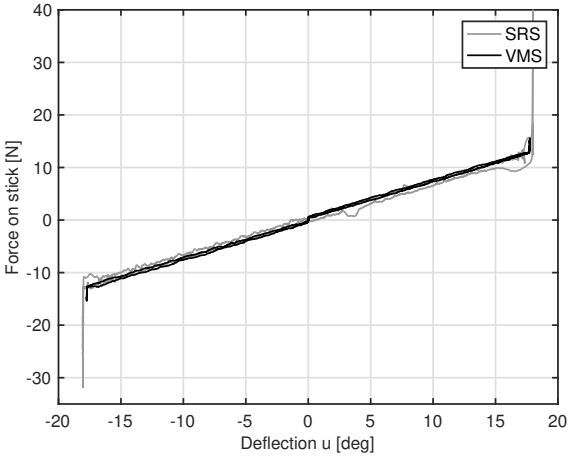

Figure 13: Force-displacement relation of the side sticks of both simulators

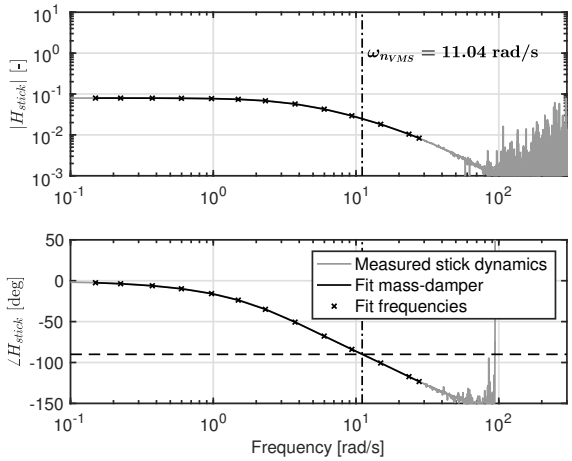

Figure 14: SRS frequency sweep compared to $\omega_{n_{VMS}}$

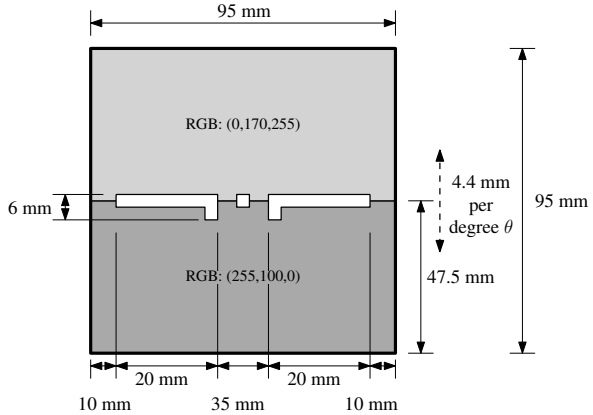

Figure 15: The dimensions of the primary flight display

Table 5: Overview of side stick settings

Parameter	Unit	Set value
Max deflections	deg	$\pm$ 18.0
Force gradient	N/deg	0.6987
Breakout force	N	0.0
Stick damping	Ns/deg	0.1747
Stick inertia	Ns^2/deg	0.0057
Stick natural frequency	rad/s	11.04

III.C. Visual System

In order to eliminate the effects of different out-of-the-window visual systems and in order to simplify the replication of the experiment, only head-down displays were used. The display graphics on the head-down displays were generated

from the same C/OpenGL code. The size of the visuals on the screen was measured and adjusted such that the artificial horizon shown on the SRS replicated the one shown in the VMS, in terms of its dimensions and movement during the experiment runs. Figure 15 shows the dimensions of the PFD on the screen.

In a previous simulator comparison, the dynamics of the displays were modelled as pure time delays.[29] The time delay in the visual system of the VMS was measured using the Image Dynamic Measurement System (IDMS)[46] and was found to be 36.3ms. The IDMS is based on detecting a change from black to white on the screen. It uses an instrument with a video input that measures the time it takes between the command being generated and the change to happen on the display. The total time delay of SRS was measured using the Visual Delay Measurement System (VDMS).[47] The VDMS test is based on a sinusoidal input signal on the pitch angle. The image on the head-down display was compared to a reference image, that was provided to a human observer through shutter glasses which sampled at twice the sinusoid frequency. The shutter glasses have a known, constant and small time delay. The observers adjusted the shutter glasses' time delay until the head-down display image and the image through the shutter glasses coincided. This was repeated for three frequencies (2, 4 and 8Hz). Two different observers performed the procedure, resulting in an estimated visual delay of approximately $33 - 39$ms. Because this fell within the same range of the VMS visual time delay, no adjustments were needed to match both simulators.

Furthermore, the dimensions of the cockpit, the ERP in relation to the head-down display and the position of the chair in relation to the side stick were compared. The only relevant difference was a vertical offset in the position from the ERP to the screen: the SRS ERP was 5 cm higher to the bottom of the screen, compared to the VMS, as can be seen in Figure 8 and 9. No correction for this offset was made.

III.D. Hypotheses

The experiment was repeated on two simulators, with considerable effort to match the cues the pilots perceived from the different simulator systems: the motion response of the simulators was equalized, the side sticks were verified to have equivalent characteristics, and the visual displays were matched. Furthermore, the task was the same. On top of the three motion filter hypotheses from Section II.F, two hypotheses on the effects of the different simulators were proposed:

H4: **No differences in absolute value of dependent measures** - Because the pilot population was similar in characteristics (type, experience, age) and size, it was hypothesized that both experiments would deliver the same results between simulators, in terms of the dependent variables considered for each experimental condition separately.

H5: **No differences in relative trends between conditions** - Similarly to hypothesis H4, it was hypothesized that the pilot control behavior data collected in both simulators would show the same relative effects between the different tested motion conditions.

IV. Results

Because the experiment featured two sets of hypotheses, two separate statistical analyses were performed. Section IV.A explains the purpose of these two statistical analyses. The following sections present the results of the tracking performance and control activity, the pilot model parameters and the open-loop parameters, respectively.

IV.A. Statistical Analysis

The first statistical test focused on the effects across the two simulators, while the second statistical test focused on the effects of motion filter order O_{mf} and motion filter frequency ω_{mf}.

IV.A.1. Statistical Analysis for Differences Across Simulators

Firstly, a two-way mixed ANOVA was performed to detect statistically significant interactions between the used simulator and motion condition, as well as the main effects of motion condition and simulator for each dependent measure. In this statistical test, a significant interaction implied that the differences between motion conditions were not the same in both simulators and hence different relative trends were present in the data. The main effect of simulator considered each condition individually to see if there was a bias between the results.

The ANOVA assumptions were tested as follows. Firstly, for the ANOVA assumption regarding outliers, the studentized residuals were used to check if data were within $\pm$ 3 standard deviations. Secondly, the Shapiro-Wilk test

was used to assess the normality of the data ($p > 0.05$). Thirdly, to assess the assumption of homogeneity of variance Levene's test of equality of error variances ($p > 0.05$) was used. Fourthly, the assumption of similarity of covariance was tested with Box's test of equality of covariance matrices ($p < 0.001$). Fifthly, Mauchly's test of sphericity was used to test the assumption of sphericity ($p > 0.05$).

The ANOVA is considered robust against violations of the assumption of normality[48] and the assumption of homogeneity of variance.[49] However in some of the dependent measures the violations were considered too severe to ignore and a non-parametric equivalent to a two-way mixed ANOVA was used. The Shreirer-Ray-Hare extension of the Kruskall-Wallis (SRH-KW) test[50,51] was used in case the assumption of normality was violated in at least four out of sixteen cases or the assumption of homogeneity of variances was violated in three out of eight cases or more. This non-parametric test assumed an equal number of participants in both simulator groups. If a significant difference between simulators was present, post-hoc Mann-Whitney U tests were performed to detect the conditions from which this difference originated. The purpose was to assess whether a single condition, or set of conditions, repeatedly gave rise to these simulator differences. No post-hoc tests to further investigate significant differences across motion conditions were performed, as this was the focus of the second statistical analysis. Table 6 presents the results of the statistical analysis for the differences across the simulators, including the test that was used.

IV.A.2. Statistical Analysis for Effects of Motion Filter Order O_{mf} and Motion Filter Frequency ω_{mf}

Following the statistical tests for the differences across simulators, a two-way repeated measures ANOVA was performed twice on the experiment data of C1 to C6: once for the VMS data and once for the SRS data. This division was made because the first statistical analysis indicated offsets in the results across the simulators, see Table 6.

In case the assumption of normality was violated in three out of six conditions or more for either the VMS or the SRS data, the SRH-KW test was used for both simulators. The interaction term $O_{mf} \times \omega_{mf}$ indicated whether the value of either O_{mf} or ω_{mf} influenced the effect of the other. Table 7 presents the results of the second statistical analysis.

In the following section, the dependent variables are presented on either boxplots or 95% confidence interval plots, depending on statistical test that was performed. In all plots, both the means and medians are indicated, as circles and horizontal dashes, respectively. The means of medians of condition C7 were used as baseline for the prediction equations. Where no mention is made of the ANOVA assumptions in the following section, all assumptions were met.

IV.B. Performance and Control Activity

Figure 16 shows pilot tracking performance in terms of RMS_e. Both simulators showed similar differences in tracking performance over the different motion conditions, which is supported by an insignificant interaction term, as can be seen in Table 6. Best tracking performance was seen in the full-motion condition C7. As expected, a significant increase was observed in RMS_e with increasing motion filter order O_{mf} of around 8% and 5% on average per motion filter order for the VMS and SRS, respectively. Furthermore, with increasing ω_{mf}, RMS_e increased significantly by 8% and 6% on average for the VMS and SRS, respectively, as can be seen in Table 7. Both in the VMS and SRS data, the $\omega_{mf} = 2.0$ rad/s conditions showed a four times larger decrease in performance with increasing motion filter order than the $\omega_{mf} = 0.5$ rad/s conditions, as also indicated by the significant interaction between motion filter order and ω_{mf}, see Table 7. There were significant differences between the simulators, as can be seen in Table 6. Post-hoc Mann Whitney U tests indicated that only in condition C4 and C7 the difference between simulators was statistically significant.

Figure 17 shows the pilot control activity in terms of RMS_u. The data showed violations of the assumption of normality in seven conditions, as well as six violations of the assumption equality of variances. In both the VMS and SRS the same relative difference between motion conditions could be seen: the interaction of simulator and motion condition was not significant, as can be seen in Table 6. In the no-motion condition C0 the median of the data was lowest, for both simulators. In the full-motion condition C7, the median was highest, indicating that pilots controlled more actively in this condition. However, according to the non-parametric statistical test, the main effect of motion condition was not significant, see Table 6. This was supported by the second statistical analysis: no significant effect of filter order O_{mf} or filter frequency ω_{mf} on the control activity was detected for the VMS or the SRS, see Table 7. There were significant differences between the two simulators. The VMS data showed a significantly larger range of RMS_u, as indicated by the taller boxplots in Figure 17: the data of the VMS contained four pilots that controlled with larger control inputs. Post-hoc Mann-Whitney U tests indicated that for all conditions a significant difference in RMS_u between the two simulators was present, which supported this finding.

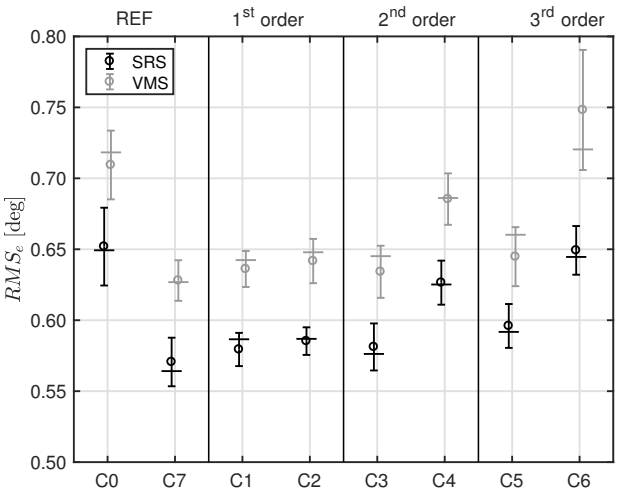

Figure 16: Pilot tracking performance

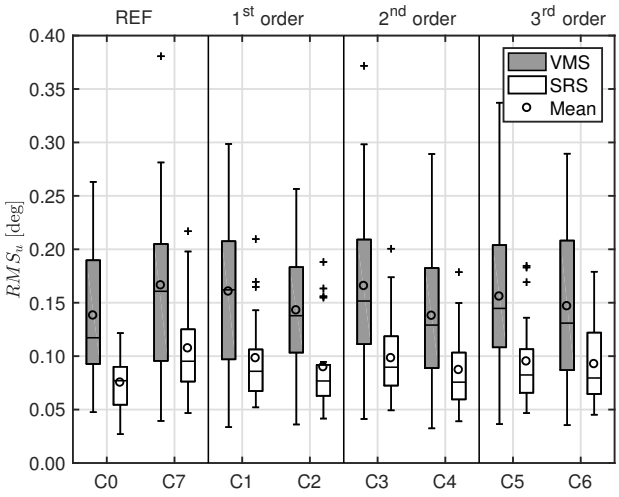

Figure 17: Pilot control activity

IV.C. Pilot Model Parameters

For each estimated pilot model, the VAF was calculated to assess the quality of the estimation. A VAF of 100% signifies that the corresponding pilot model was able to perfectly explain all the variance in the pilot control signal u. Figure 18 shows the VAF. It can be seen that values range from 70% to 92%. In previous experiments similar VAF values were found.[34,52]

Figure 19 shows the variance of the output signal of the motion pilot model $\sigma^2_{u_m}$ over the variance of the output signal of the visual pilot model $\sigma^2_{u_v}$ as a measure of how much motion was used by the pilots. A higher variance fraction signifies more motion used. A variance fraction of 100% indicates that the variance of the motion and visual signals are equal. The values ranged from 100.4% in C7 to 0% in motion condition C6. For the no-motion condition C0 no data was available, because the motion channel of the pilot model was not estimated for C0 (see Section II.E). Both the VMS and SRS data violated the ANOVA assumption of normality for three motion conditions. Both simulators showed similar trends in the data, as illustrated by an insignificant interaction between simulator and motion condition, see Table 6. A significant decrease in motion channel usage with increasing filter frequency ω_{mf} was found, see Table 7. For the VMS the average decrease was 65% and for the SRS the average decrease was 70%, for the change from $\omega_{mf} = 0.5$ rad/s to $\omega_{mf} = 2.0$ rad/s, over the three filter orders. Furthermore, the data showed a decrease in $\sigma^2_{u_m}/\sigma^2_{u_v}$ with increasing motion filter order O_{mf} for the $\omega_{mf} = 2.0$ rad/s conditions, which averaged at 31% for the VMS and 41% for the SRS per filter order. For the $\omega_{mf} = 0.5$ rad/s conditions no change was seen with increasing O_{mf}. Although this was visible in the data, no significant main effect of motion filter order O_{mf} was found in either simulator, see Table 7. Furthermore, the interaction between ω_{mf} and filter order O_{mf} was insignificant, see Table 7. There were significant differences between the VMS and SRS within single conditions, as indicated by the significant main effect of simulator, see Table 6. Post-hoc Mann-Whitney U tests indicated that for conditions C4 and C6 the data was significantly different. In Figure 19 these two conditions are the only ones where the median of the SRS data falls below the first quartile of the VMS data.

Figure 20 shows the pilot model visual gain K_v. A higher K_v indicates that pilots responded with larger inputs to visual cues. The data severely violated the assumption of normality, as well as the assumption of equality of error variances, in 12 and 5 cases in total, respectively. No significant interaction between simulator and motion filter condition was found: both simulators showed similar relative differences between conditions, see Table 6. No significant main effect of motion filter order O_{mf} was found, see Table 7. The interaction between O_{mf} and ω_{mf} was not found to be significant for both simulators either. However, for both simulators a significant decrease in median K_v with increasing ω_{mf} was found, of 19% and 13% average, for the VMS and SRS, respectively, over the three filter orders. There were significant differences between the VMS and SRS, as indicated by a significant main effect of simulator, see Table 6. Two VMS pilots had notably higher visual gains. Both these pilots also belonged to the group of four VMS pilots with notably higher RMS_u and in C1 and C4 their effect was significant, as assessed with post-hoc Mann Whitney U tests. In the no-motion condition C0, the two simulators showed similar medians ($K_{v_{VMS}} = 0.0437$ and $K_{v_{SRS}} = 0.0431$), indicating that with no motion present, pilots controlled with similar gains in both the VMS and SRS. In both simulators, the prediction equations from Ref. 13 supported the results, with correlation coefficients

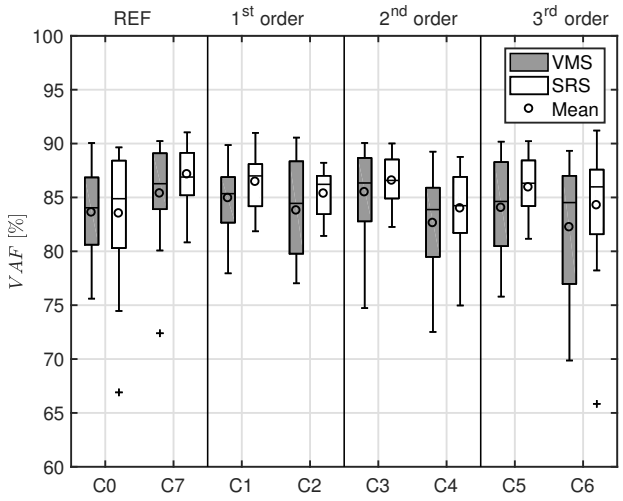

Figure 18: Pilot model variance accounted for

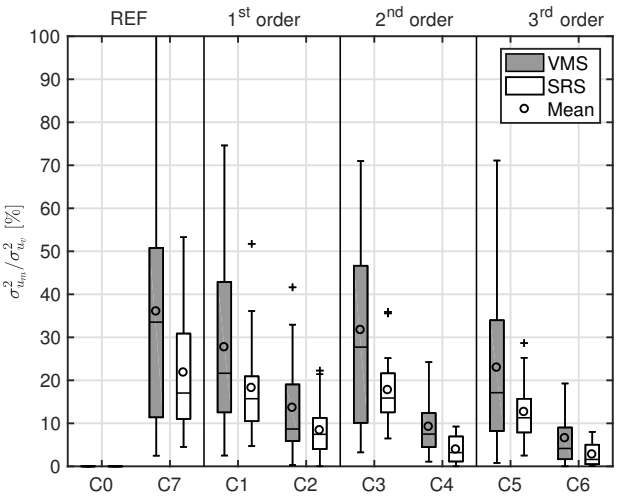

Figure 19: Variance of visual over motion control signal

of $\rho = 0.83$ and $\rho = 0.91$ for the VMS and SRS, respectively. The equations predicted the trends in the SRS results of K_v well. The largest difference between the experimental results and predicted K_v was 8.9%. The VMS data showed higher medians than predicted for most conditions, apart from C0 and C6 where the median K_v of the experiment data was found below the predicted value $\hat{K}_v$.

Figure 21 shows the pilot model motion gain K_m. A higher K_m indicates that pilots responded with larger inputs to motion cues. The assumption of equality of error variances was violated in all but two conditions. Like the visual pilot model gain K_v, the motion gain K_m displayed similar relative trends over the motion conditions for both simulators: the interaction between simulator and motion condition was insignificant, see Table 6. However, the main effect of simulator was significant. Post-hoc Mann-Whitney U tests indicated a difference in distribution for C4. The VMS data of K_m did not reveal any significant change with increasing filter order O_{mf}, see Table 7. However, the SRS data did show an average 20% significant decrease in K_m with increasing filter order O_{mf} in the $\omega_{mf} = 2.0$ rad/s conditions. A significant interaction between O_{mf} and ω_{mf} was observed in the SRS data, where K_m in the $\omega_{mf} = 2.0$ rad/s conditions decreased almost 3 times more over the three filter orders than in the $\omega_{mf} = 0.5$ rad/s conditions, in contrast to the VMS data where no significant interaction was found. Both the VMS and SRS data showed a significant decrease in K_m with increasing ω_{mf}, meaning that pilots responded less to motion information in the $\omega_{mf} = 2.0$ rad/s conditions.

Figure 22 shows the pilot model visual lead time constant T_L. A higher lead time constant indicates that pilots use more visual cues to generate lead to control the aircraft. The only violation of the ANOVA assumptions was due to outliers: the data showed four outliers in one VMS pilot and one outlier in an SRS pilot. An ANOVA was performed with and without the outliers, which produced the same results. Therefore, the outliers were left in the dataset. The data of both simulators showed similar trends, with little differences between the simulators: no significant interaction between simulator and motion condition was observed, see Table 6. A significant increase in visual lead time T_L with increasing O_{mf} was found in both simulators, see Table 7. Like RMS_e and K_m, this effect was mostly visible in the $\omega_{mf} = 2.0$ rad/s conditions, which increased by 23% and 12% on average for the three filter orders, for the VMS and SRS, respectively. Furthermore, both simulators also showed a significant increase in T_L with increasing ω_{mf}, of 35% and 20% on average. The VMS data did not show a significant interaction between O_{mf} and ω_{mf}, whereas the SRS data did, see Table 7. No significant differences between the two flight simulators were found, as indicated by an insignificant main effect of simulator, see Table 6. The prediction equations supported the results, correctly indicating the trends of increasing T_L for increasing ω_{mf} and O_{mf} for both the VMS and SRS, with correlation coefficients of $\rho = 0.86$ and $\rho = 0.95$, respectively. In both C0 and C6 the prediction equations estimated $\hat{T}_L$ to be lower than the experimental results, mirroring what was seen for the prediction equations of $\hat{K}_v$. In the no-motion condition C0 the means of the data of both simulators were found at the inverse of the short period frequency of the controlled dynamics: $1/\omega_{sp} = 1/0.6892$ rad/s $= 1.4509$ s, with little difference between them.

The three equalization parameters together showed that mainly for the higher filter frequency $\omega_{mf} = 2.0$ rad/s (conditions C2, C4 and C6) the pilots controlled with smaller gains and used more visual information to generate lead for larger filter orders O_{mf}, even though the statistical analysis did not support this completely, see Table 6 and Table 7. The following four parameters are the limitation parameters. The limitation parameters showed that pilots' frequency

response was more damped and more of the frequency response was attenuated by the neuromuscular system for higher O_{mf}, once again mainly in the $\omega_{mf} = 2.0$ rad/s conditions.

Figure 23 shows the pilot model visual time delay τ_v. The ANOVA showed no significant interaction between simulator and motion condition, see Table 6. A significant difference between simulators for conditions C3, C5, C6 and C7 was present, as indicated by post-hoc Mann-Whitney U tests. However, the data of both simulators did not show significant main effects of motion condition, see Table 6. This was supported by the second statistical analysis. The data did not reveal any significant effect of O_{mf} or ω_{mf} for neither of the two simulators, see Table 7. Furthermore, no significant interaction between O_{mf} and ω_{mf} was found. However, the prediction equations did estimate there would be effects visible, see Figure 23. The predictions correlated to the VMS and SRS data with $\rho = -0.03$ and $\rho = -0.79$, respectively. Hence, the predictions of $\hat{\tau}_v$ were not supported by the results of the current experiment.

Figure 24 shows the pilot model motion time delay τ_m. Like the visual time delay τ_v, the motion time delay τ_m remained relatively constant over the different motion conditions. Compared to previous studies,[34] the values found in C4 and C6 were disproportionately high, which indicated that in these conditions τ_m could not be estimated accurately. In Ref. 53, a similar situation was encountered. The motion time delay showed little to no difference over the other conditions or between simulators. The SRS data violated the assumption of normality in all conditions and the VMS violated this assumption in 2 conditions. The non-parametric statistical test confirmed the findings: no significant effects were found, see Table 6. The second statistical test was not performed.

Figure 25 shows the neuromuscular damping constant ζ_{nm}. A smaller ζ_{nm} indicates that the pilot model frequency response is less damped. In both simulators similar trends were present, see Table 6. A significant increase in ζ_{nm} for increasing filter order O_{mf} was found, see Table 7. This average increase of 11% and 5% in the VMS and SRS, respectively, was visible only in the $\omega_{mf} = 2.0$ rad/s conditions. The $\omega_{mf} = 0.5$ rad/s conditions did not show an increase. Hence, for both simulators there was a significant interaction between O_{mf} and ω_{mf}, see Table 7. Furthermore, both simulators showed a significant increase in ζ_{nm} with increasing ω_{mf}, see Table 7: in the VMS ζ_{nm} increased by 17% and in the SRS by 15% on average. The difference of 0.12 in ζ_{nm} in the no-motion C0 indicated that the motion was not the source of the differences across simulators, but the other systems of which the pilots received cues, such as the side stick or the visuals. Finally, the main effect of simulator was significant, indicating that differences between the simulators were present, see Table 6. Post-hoc Mann-Whitney U tests subsequently indicated that for all conditions, except C5 and C6, there were differences between the simulators.

Figure 26 shows the neuromuscular frequency ω_{nm}. A smaller ω_{nm} indicates that the pilot model neuromuscular system attenuated a smaller bandwidth of the frequency response. The data of the VMS and SRS showed the same trends: no significant interaction was found between simulator and motion condition and there were also no significant differences between the two simulators, see Table 6. The data did not show any significant effect of ω_{mf} or O_{mf} in the SRS data, see Table 7. However, the VMS data did show a significant increase in ω_{nm} with increasing ω_{mf}. No significant interactions between O_{mf} and ω_{mf} were found. The prediction equations predicted opposite trends than the data showed: they correlated to the VMS and SRS data with $\rho = -0.79$ and $\rho = -0.71$, respectively. Hence, the prediction equation of $\hat{\omega}_{nm}$ was not supported by the results of the current experiment.

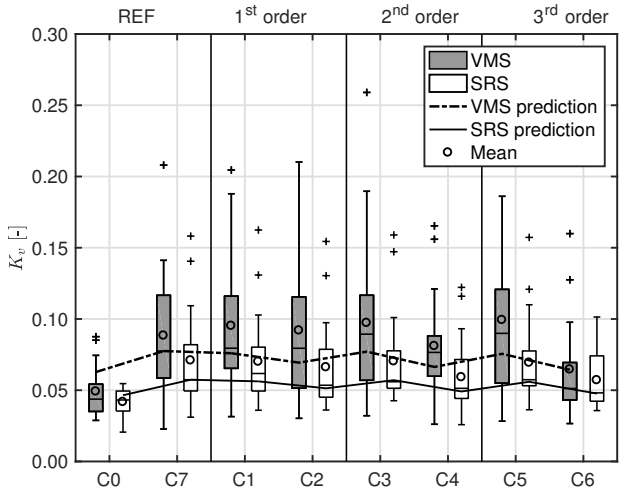

Figure 20: Pilot model visual gain K_v

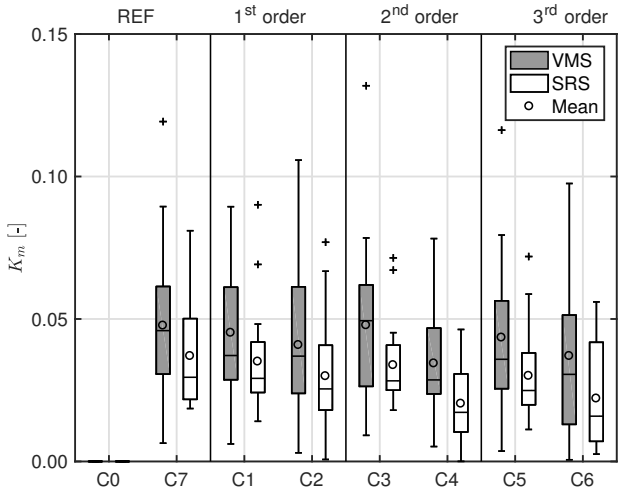

Figure 21: Pilot model motion gain K_m

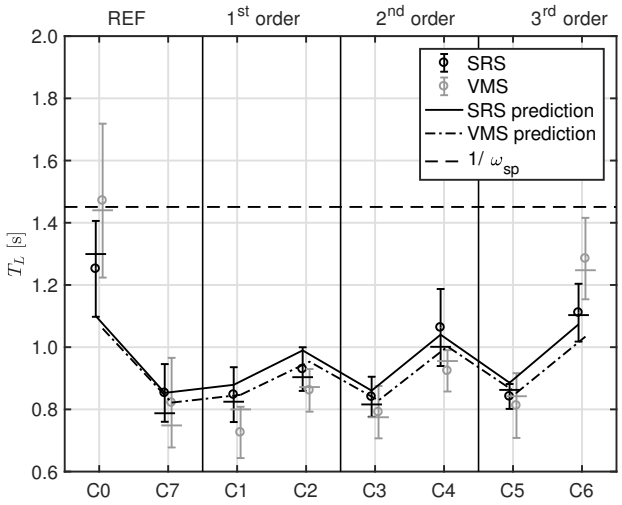

Figure 22: Pilot model lead time constant T_L

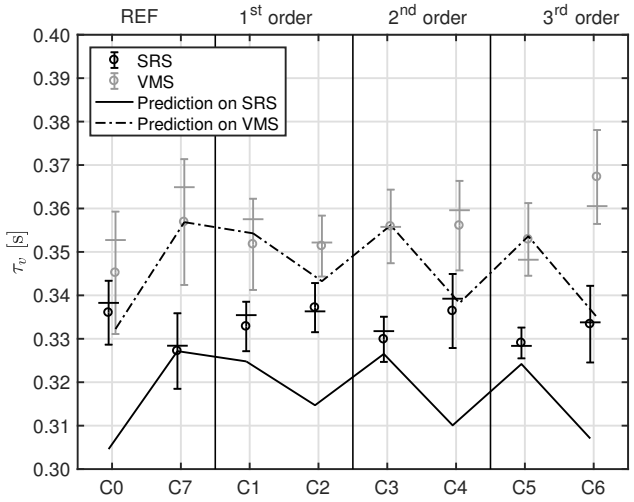

Figure 23: Pilot model visual time delay τ_v

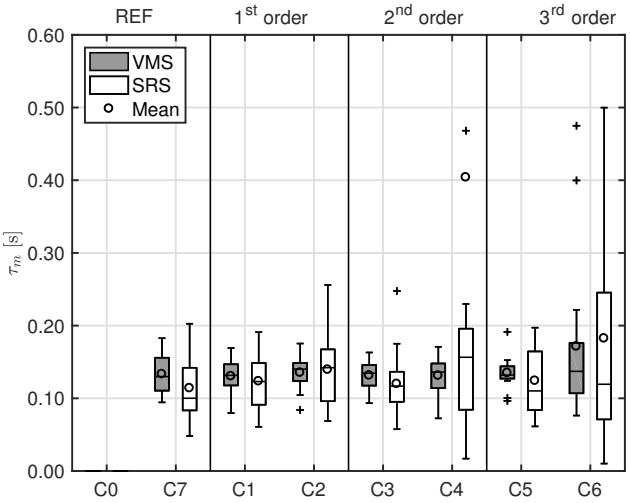

Figure 24: Pilot model motion time delay τ_m

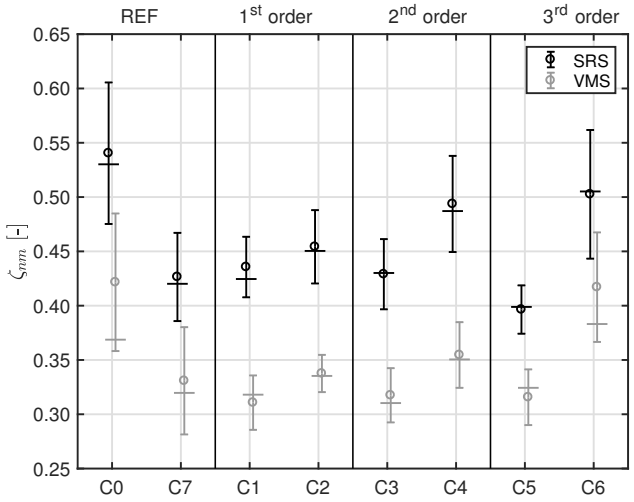

Figure 25: Pilot model neuromuscular damping ζ_{nm}

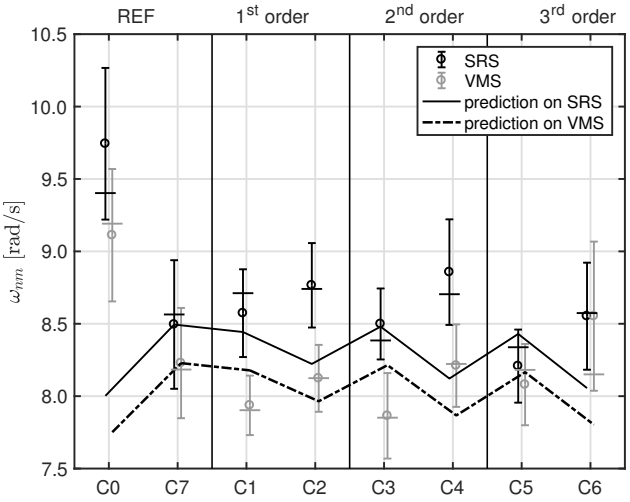

Figure 26: Pilot model neuromuscular frequency ω_{nm}

IV.D. Open-loop Dynamics

The closed-loop tracking task that was performed in this experiment was a combined target-following and disturbance-rejection task. Performance depended on attenuating errors caused by both the target and disturbance forcing functions.[54] Overall, as can be seen in Figures 27 to 30, the values of the open-loop parameters found in this experiment were similar to previous research, Ref. 34 for example.

Figure 27 shows the open-loop target crossover frequency $\omega_{c,t}$. The SRS data violated the assumptions of normality in three conditions. The same trends were observed in both simulators: no significant interaction was found between the effects of simulator and motion condition, see Table 6. Also no significant difference between simulators was present, see Table 6. In both simulators, no significant change in $\omega_{c,t}$ with increasing O_{mf} was found, see Table 7. Furthermore, no significant interaction between O_{mf} and ω_{mf} was found. However, both simulators showed an average significant increase of 19% in $\omega_{c,t}$ from the $\omega_{mf} = 0.5$ rad/s conditions to the $\omega_{mf} = 2.0$ rad/s conditions.

Figure 28 shows the open-loop disturbance crossover frequency $\omega_{c,d}$. The data of $\omega_{c,d}$ violated the assumption of normality in 5 cases in total. The SRH-KW test indicated a significant interaction between simulator and motion condition on $\omega_{c,d}$, as can be seen in Table 6. The data of the two simulators showed the same trends, except for the difference between C5 and C6, see Figure 28. The medians of $\omega_{c,d}$ of the SRS data decreased 7.0% more from C5 to C6 (third order conditions), as compared to the VMS data. With these two conditions excluded, the SRH-KW test did not return a significant interaction effect. Because the second largest difference in trends was a 5.8% larger increase in $\omega_{c,d}$ from C0 to C7 in the VMS data, the significant interaction between simulator and motion condition was not considered relevant for the results. No significant main effect of O_{mf} was found, see Table 7. Both simulators did show a significant average decrease of 15.6% and 11.5%, for the VMS and SRS, respectively, with the increase from $\omega_{mf} = 0.5$ rad/s to $\omega_{mf} = 2.0$ rad/s. Furthermore, the main effect of simulator was significant, indicating that there were differences between the simulators, see Table 6. A post-hoc Mann-Whitney U test indicated that this difference originated from C0, similar to what was seen in the data of ζ_{nm} and ω_{nm}. The prediction equations from Ref. 13 supported the experimental results, showing similar trends for both simulators, with strong correlations of $\rho = 0.94$ for both simulators.

Figure 29 shows the open-loop target crossover phase margin $\varphi_{m,t}$. Both simulators showed similar trends in the data: no significant interaction between simulator and motion condition on $\varphi_{m,t}$ was found, see Table 6. In both simulators the data showed a significant decrease with increasing O_{mf}: over the three filter orders $\varphi_{m,t}$ decreased on average 6.1% and 6.9% for the VMS and SRS, respectively. Furthermore, with increasing ω_{mf}, the $\varphi_{m,t}$ decreased significantly as well in both simulators: on average 26% in the VMS and 23% in the SRS for the change from $\omega_{mf} = 0.5$ rad/s to $\omega_{mf} = 2.0$ rad/s. The interaction between O_{mf} and ω_{mf} was only significant in the SRS, however, see Table 7. The main effect of simulator was significant, see Table 6, as $\varphi_{m,t}$ was consistently slightly lower for the VMS data.

Figure 30 shows the open-loop disturbance crossover phase margin $\varphi_{m,d}$. No significant interaction between simulator and motion filter was found, see Table 6, which indicated that the similar trends were present in the data. The disturbance crossover phase margin $\varphi_{m,d}$ showed a significant decrease for increasing O_{mf}, see Table 7. This effect was mainly visible in the $\omega_{mf} = 2.0$ rad/s conditions, with a decrease of around 10% per motion filter order for both simulators. In the $\omega_{mf} = 0.5$ rad/s conditions $\varphi_{m,d}$ remained constant. Hence, for both simulators the interaction between O_{mf} and ω_{mf} was significant, see Table 7. Both simulators also showed a significant decrease in $\varphi_{m,d}$ for increasing ω_{mf}, of around 15% and 10%, for the VMS and SRS respectively. This result was opposed by the prediction equations, which predicted a slight increase in $\varphi_{m,d}$ for increasing ω_{mf}. The correlation coefficients confirmed this finding: for the VMS $\rho = -0.77$ and for the SRS $\rho = -0.84$. The prediction equations did not support the results of this experiment. Finally, a significant difference between simulators was found, see Table 6. Post-hoc Mann-Whitney U tests indicated that these differences could be found in C1, C3 and C5.

The combination of open-loop parameters indicated a decrease in motion channel use for both increasing ω_{mf} and increasing O_{mf} in the open-loop response. Most notably, the decreasing $\omega_{c,d}$ and decreasing $\varphi_{m,t}$ reflected this, as well as the increasing $\omega_{c,t}$.

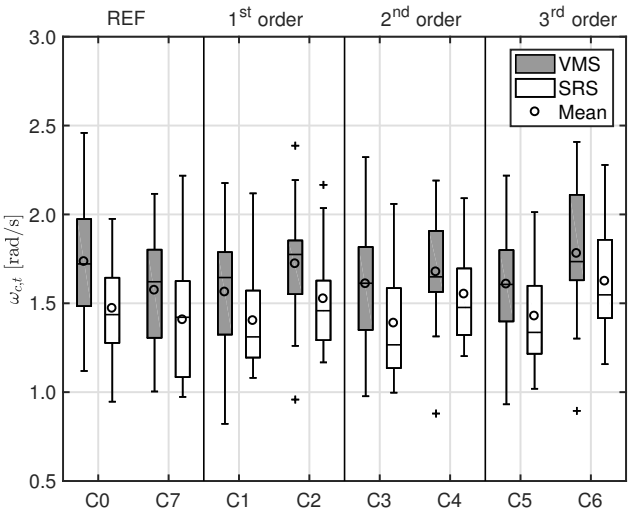

Figure 27: Open-loop target crossover frequency $\omega_{c,t}$

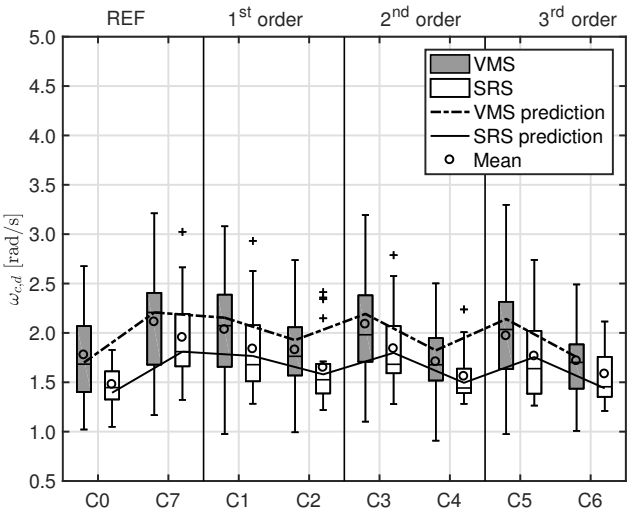

Figure 28: Open-loop disturbance crossover frequency $\omega_{c,d}$

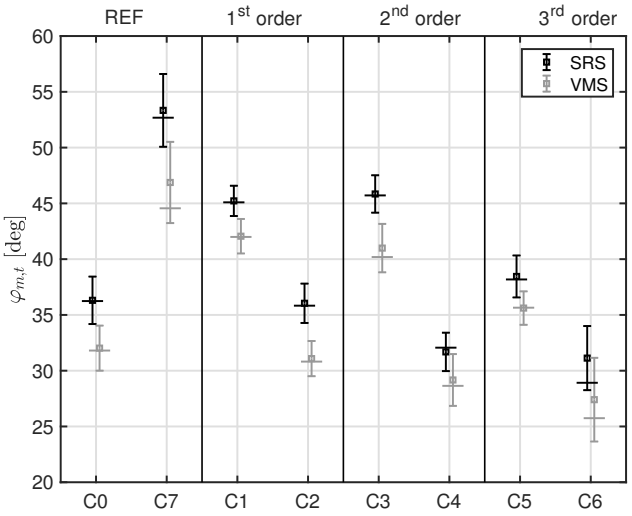

Figure 29: Open-loop target phase margin $\varphi_{m,t}$

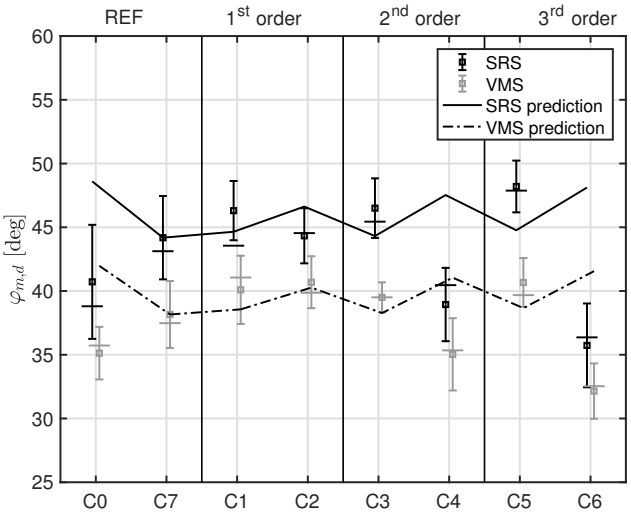

Figure 30: Open-loop disturbance phase margin $\varphi_{m,d}$

Table 6: Summary of statistical analysis for simulator differences

		Simulator			Motion condition			Simulator × Motion condition		
	Test	*df*	*F*	*p*	*df*	*F*	*p*	*df*	*F*	*p*
RMS_e	ANOVA	1.0, 32.0	0.184	0.031	3.2, 102.6^{gg}	26.657	<0.001	3.2, 102.6^{gg}	0.957	0.420
RMS_u	SRH-KW	1.0, 256.0	55.006	<0.001	7.0, 256.0	4.602	0.121	7.0, 256.0	0.719	0.081
$\sigma^2_{u_m}/\sigma^2_{u_v}$	SRH-KW	1.0, 256.0	12.339	<0.001	7.0, 256.0	92.062	<0.001	7.0, 256.0	1.417	0.062
K_v	SRH-KW	1.0, 256.0	19.371	<0.001	7.0, 256.0	41.357	<0.001	7.0, 256.0	1.915	0.052
K_m	SRH-KW	1.0, 237.0	21.187	<0.001	6.0, 237.0	18.051	0.002	6.0, 237.0	1.278	0.054
T_L	ANOVA	1.0, 32.0	0.006	0.938	2.7, 91.4^{gg}	26.624	<0.001	2.7, 91.4^{gg}	2.632	0.061
τ_v	ANOVA	1.0, 32.0	6.76	0.014	4.5,143.6^{gg}	0.975	0.429	4.5, 143.6^{gg}	1.491	0.202
τ_m	SRH-KW	1.0, 237.0	1.537	0.149	6.0, 237.0	6.600	0.100	6.0, 237.0	3.998	0.135
ζ_{nm}	ANOVA	1.0, 32.0	6.34	0.017	3.5, 118.8^{gg}	8.591	<0.001	3.5, 118.8^{gg}	0.507	0.706
ω_{nm}	ANOVA	1.0, 32.0	0.773	0.386	4.1,131.5^{gg}	9.591	<0.001	4.1,131.5^{gg}	1.017	0.347
$\omega_{c,t}$	ANOVA	1.0, 32.0	4.143	0.051	3.9, 124.8^{gg}	21.239	<0.001	3.9, 124.8^{gg}	1.114	0.352
$\omega_{c,d}$	SRH-KW	1.0, 256.0	21.992	<0.001	7.0, 256.0	28.428	<0.001	7.0, 256.0	0.767	0.009
$\varphi_{m,t}$	ANOVA	1.0, 32.0	1139.7	0.034	3.4, 108.9^{gg}	77.521	<0.001	3.4, 108.9^{gg}	0.794	0.514
$\varphi_{m,d}$	ANOVA	1.0, 32.0	1809.8	0.02	4.3, 138.3^{gg}	14.04	<0.001	4.3, 138.3^{gg}	0.702	0.602

gg = Greenhouse-Geisser correction
■ = significant ($p < 0.050$)
□ = not significant ($p \geq 0.050$)

Table 7: Summary of statistical analysis for motion filter effects

VMS

		O_{mf}			ω_{mf}			$O_{mf} \times \omega_{mf}$		
	Test	*df*	*F*	*p*	*df*	*F*	*p*	*df*	*F*	*p*
RMS_e	ANOVA	1.5, 23.8^{gg}	21.866	<0.001	1.0, 16.0	18.302	<0.001	1.5, 23.8^{gg}	7.045	0.007
RMS_u	SRH-KW	2.0, 96.0	0.066	0.484	1.0, 96.0	1.317	0.180	2.0, 96.0	0.243	0.443
$\sigma^2_{u_m}/\sigma^2_{u_v}$	SRH-KW	2.0, 96.0	3.691	0.079	1.0, 96.0	23.903	<0.001	2.0, 96.0	0.529	0.384
K_v	SRH-KW	2.0, 96.0	2.416	0.149	1.0, 96.0	3.651	0.034	2.0, 96.0	1.984	0.185
K_m	ANOVA	2.0, 32.0	0.781	0.467	1.0, 16.0	11.862	0.003	2.0, 32.0	1.505	0.237
T_L	ANOVA	2.0, 32.0	34.842	<0.001	1.0, 16.0	34.186	<0.001	2.0, 32.0	6.740	0.444
τ_v	ANOVA	2.0, 32.0	1.778	0.185	1.0, 16.0	1.438	0.248	2.0, 32.0	1.670	0.204
τ_m	SRH-KW	2.0, 96.0	0.327	0.425	1.0, 96.0	0.400	0.516	2.0, 96.0	0.207	0.451
ζ_{nm}	ANOVA	1.4, 21.7^{gg}	5.915	0.015	1.0, 16.0	14.814	0.001	1.4,21.7^{gg}	3.998	0.047
ω_{nm}	ANOVA	2.0, 32.0	2.233	0.124	1.0, 16.0	7.136	0.017	2.0, 32.0	0.379	0.688
$\omega_{c,t}$	SRH-KW	2.0, 96.0	0.263	0.438	1.0, 96.0	4.544	0.019	2.0, 96.0	0.279	0.435
$\omega_{c,d}$	SRH-KW	2.0, 96.0	0.750	0.344	1.0, 96.0	8.1097	0.002	2.0, 96.0	0.743	0.345
$\varphi_{m,t}$	ANOVA	2.0, 32.0	15.62	<0.001	1.0, 16.0	55.507	<0.001	2.0, 32.0	2.181	0.129
$\varphi_{m,d}$	ANOVA	2.0, 32.0	9.737	<0.001	1.0, 16.0	12.923	0.002	2.0, 32.0	8.324	0.001

SRS

		O_{mf}			ω_{mf}			$O_{mf} \times \omega_{mf}$		
	Test	*df*	*F*	*p*	*df*	*F*	*p*	*df*	*F*	*p*
RMS_e	ANOVA	2.0, 32.0	22.592	<0.001	1.0, 16.0	17.972	<0.001	2.0, 32.0	7.346	0.002
RMS_u	SRH-KW	2.0, 96.0	$6.05{\cdot}10^{-04}$	0.500	1.0, 96.0	1.069	0.2261	2.0, 96.0	0.578	0.375
$\sigma^2_{u_m}/\sigma^2_{u_v}$	SRH-KW	2.0, 96.0	6.095	0.024	1.0, 96.0	46.283	<0.001	2.0, 96.0	2.297	0.159
K_v	SRH-KW	2.0, 96.0	0.902	0.319	1.0, 96.0	4.952	0.015	2.0, 96.0	0.703	0.352
K_m	ANOVA	2.0, 32.0	7.44	0.002	1.0, 16.0	27.328	<0.001	2.0, 32.0	6.305	0.005
T_L	ANOVA	2.0, 32.0	4.164	0.045	1.0, 16.0	13.208	0.002	2.0, 32.0	4.328	0.027
τ_v	ANOVA	2.0, 32.0	0.717	0.496	1.0, 16.0	2.249	0.153	2.0, 32.0	0.052	0.949
τ_m	SRH-KW	2.0, 96.0	0.043	0.489	1.0, 96.0	2.442	0.075	2.0, 96.0	0.012	0.497
ζ_{nm}	ANOVA	2.0, 32.0	0.392	0.618	1.0, 16.0	15.193	<0.001	2.0, 32.0	2.924	0.070
ω_{nm}	ANOVA	2.0, 32.0	2.281	0.119	1.0, 16.0	3.266	0.09	2.0, 32.0	0.254	0.777
$\omega_{c,t}$	SRH-KW	2.0, 96.0	0.975	0.307	1.0, 96.0	9.334	0.001	2.0, 96.0	0.253	0.441
$\omega_{c,d}$	SRH-KW	2.0, 96.0	0.329	0.424	1.0, 96.0	6.726	0.005	2.0, 96.0	0.532	0.383
$\varphi_{m,t}$	ANOVA	2.0, 32.0	23.524	<0.001	1.0, 16.0	91.859	<0.001	2.0, 32.0	5.366	0.010
$\varphi_{m,d}$	ANOVA	2.0, 32.0	5.145	0.025	1.0, 16.0	23.458	<0.001	2.0, 32.0	8.519	0.001

gg = Greenhouse-Geisser correction
■ = significant ($p < 0.050$)
□ = not significant ($p \geq 0.050$)

V. Discussion

This paper presents the results of a human-in-the-loop tracking experiment that was performed to evaluate the effects of varying motion filter order O_{mf} and motion filter break frequency ω_{mf} on pilot tracking performance and behavior. Whereas the effects of parameters of the motion filter on pilot control behavior and performance have been previously studied,[13,14] the filter order O_{mf} has not received the same attention. By making use of a multimodal pilot model that was fitted on time traces that were recorded in a combined target-following and disturbance-rejection task with eight different motion conditions, changes in pilot control behavior were investigated. The motion filter order O_{mf} and motion filter break frequency ω_{mf} were varied between motion conditions. To compare the results and investigate the effects of a different flight simulator, the experiment was performed in two full-motion research flight simulators, the VMS and the SRS, respectively.

V.A. Discussion of Hypotheses

It was hypothesized that with increasing filter order O_{mf}, pilots would display lower performance and less use of motion feedback in their control strategy (Hypothesis H1). Looking at RMS_e, an increase with increasing O_{mf} indicated that performance decreased. Furthermore, with increasing O_{mf}, a significant increase in T_L suggested that pilots relied more on visual cues to generate lead to control the aircraft. Both these effects were predominantly present in the higher motion filter break frequency setting $\omega_{mf} = 2.0$ rad/s. The data from the SRS experiment showed a 20% significant decrease in K_m with increasing O_{mf}, which indicated that pilots responded less to the motion signal. This effect was also visible in the data of the VMS, even with relative differences between conditions of the same magnitude. However, a larger spread between participants in the VMS data was observed and the decrease of K_m with increasing motion filter order was not found to be significant. Finally, even though in both simulators the crossover frequencies $\omega_{c,t}$ and $\omega_{c,d}$ showed an increase and decrease with increasing O_{mf}, respectively, these effects were not found to be significant. The corresponding phase margins, however, did show significant decreases of 10% per filter order, indicating the pilots controlled less stably for increasing motion filter order. Even though the fraction of control signal variances $\sigma^2_{u_m}/\sigma^2_{u_v}$ did not return any significant differences, the data did show a slight decrease for increasing motion filter order. Overall, hypothesis H1 could be accepted: pilots showed lower performance and less use of motion feedback for increasing motion filter order. This result is in line with the fidelity criteria proposed by Ref. 39 and 25 and previous experiments where motion conditions of differing fidelity were tested, Ref. 15 for example. The experimental conditions with $\omega_{mf} = 2.0$ rad/s showed larger decreases in motion fidelity using the criteria by Sinacori[39] and Schroeder[25] for increasing O_{mf}, which explained the significant interactions between O_{mf} and ω_{mf}. The motion filters themselves caused 90 degrees of phase lead for every increasing order. In the conditions with $\omega_{mf} = 2.0$ rad/s this phase distortion was present on a larger bandwidth, as compared to $\omega_{mf} = 0.5$ rad/s. Hence, it could have impacted the pilots more. This phase lead translated into the open-loop phase margins, as visible in Eq. (6) and (7). This is supported by the significant interaction between O_{mf} and ω_{mf} that was found for $\varphi_{m,t}$ and $\varphi_{m,d}$, see Table 7.

It was hypothesized that with increasing motion filter frequency ω_{mf}, pilots would show similar effects as to an increasing motion filter order O_{mf}: lower performance and less use of motion feedback in their control strategy (Hypothesis H2). Furthermore, it was expected that the effects of ω_{mf} would be stronger than the effects of motion filter order O_{mf} (Hypothesis H3). Except for RMS_u, τ_v and τ_m, all dependent measures showed a significant effect of increasing ω_{mf}. Furthermore, whereas both simulators showed an increase in ω_{nm} for increasing ω_{mf}, this was only significant in the VMS. In the data of both simulators, pilots showed a higher RMS_e with increasing ω_{mf}. Furthermore, the fraction of $\sigma^2_{u_m}/\sigma^2_{u_v}$ indicated that with increasing ω_{mf}, less use was made of motion feedback. The motion gain K_m supported this, with a similar significant decrease. The visual equalization parameters K_v and T_L showed a significant decrease and an increase for increasing ω_{mf}, respectively. This indicated that pilots used more visual cues to generate lead, while controlling with smaller gains. All four open-loop parameters showed significant effects of ω_{mf}. The increase in $\omega_{c,t}$ with increasing ω_{mf} indicated an improved target-following performance and the corresponding decrease in $\varphi_{m,t}$ signified lower stability. The decrease in $\omega_{c,d}$ with increasing ω_{mf} indicated a degraded disturbance-rejection performance and the corresponding decrease in $\varphi_{m,d}$ signified lower stability. These four parameters together indicated a decreasing dependence on the motion channel of the pilot model in the open-loop responses, with increasing ω_{mf}. Hypothesis H2 could be accepted: pilots showed a decrease in use of the motion channel and a decrease in performance with increasing ω_{mf}. This finding is consistent with previous experiments.[14,15]

Furthermore, hypothesis H3 could be accepted as well: the effects of ω_{mf} were more prevalent than O_{mf} for the chosen experimental conditions. However, it is important to realize that only two ω_{mf}'s were present in the experiment and the relative change between the two frequencies might have been more severe than the change with each order of the motion filter. The change in ω_{mf} resulted in larger differences in the dependent variables than the changes in

O_{mf}, even in the $\omega_{mf} = 2.0$ rad/s conditions where the fidelity criteria of Sinacori[39] and Schroeder[25] predicted large effects for both ω_{mf} and O_{mf}. The results indicated that a first order motion filter resulted in the best performance. However, when ω_{mf} was sufficiently low, the filter order did not influence pilot behavior. A low ω_{mf} did result in better pilot performance. Hence, to compensate for lower a ω_{mf}, a larger filter order (i.e. second or third order) could be used to prevent the simulator from drifting without causing a decrease in pilot performance.

Even though meticulous attention was paid to match the VMS and SRS, most dependent measures did show clear offsets between both simulators: Hypothesis H4 was rejected. These differences between simulators were partially caused by four VMS pilots who used substantially larger control inputs during the task, which had a direct effect on RMS_u, K_v, K_m and the open-loop parameters, and hence also on $\sigma^2_{u_m}/\sigma^2_{u_v}$. Furthermore, the differences could also be caused by the difference in side stick arm. The side stick of the VMS had a 4.9 cm longer arm, which might have prompted the pilots to control with higher a RMS_u. Furthermore, the armrest in the VMS was covered with a canvas fabric, which allowed the pilots' arm to slide freely over the armrest. The armrest in the SRS, however, was covered in artificial leather, which prevented free movement of the arm to a certain degree. The difference in ζ_{nm} in C0 supported both these theories. Finally, many of the VMS pilots had experience in tracking tasks, whereas the SRS pilots usually performed such a task for the first time. Even though training runs ensured pilots showed constant performance (as assessed with RMS_e), this difference could have also caused the VMS pilots to control with a higher RMS_u.

With a few minor exceptions, all relative trends between the different tested motion conditions were highly consistent across simulators and therefore hypothesis H5 could be accepted. The only case where a significant interaction between motion condition and simulator was found, was for the disturbance crossover frequency $\omega_{c,d}$. Although this interaction was significant, it was not found to be relevant for the results, as the interaction was due to a single pair of conditions and the difference in trend was only 1% larger than other differences between conditions which did not cause a significant interaction.

V.B. Discussion of Statistical Analysis

Even though the ANOVA is considered by some to be essentially non-parametric,[48] in several cases the violations of its assumptions were quite severe. Hence, for some of the dependent variables a different statistical test was used: the Scheirer-Ray-Hare extension of the Kruskall-Wallis test.[50,51] This test is deemed to be a viable non-parametric alternative to an ANOVA, but it is found to lack statistical power in case interaction effects other than the main effects that are being tested are present.[55] Lower statistical power translates to a higher Type-II (false negative) error probability, which could have influenced some of the conclusions, as some of the variables where this test was applied (K_v, for example) did show consistent variation across conditions, but none were found significant.

V.C. Discussion of Prediction Equations

The prediction equation equations from Ref. 13 were compared to the experimental data. The predictions of K_v, T_L and $\omega_{c,d}$ were supported very well by the results, with correlation coefficients above $\rho > 0.8$. In C0 and C6, the prediction equations indicated higher $\hat{T}_L$'s than measured in the experiment. $1/\omega_{sp}$ appeared to be a more accurate predictor for T_L in conditions where little use was made of motion feedback. The equations for τ_v, ω_{nm} and $\varphi_{m,d}$ did not predict the results of this experiment, with correlation coefficients ranging from $\rho = -0.84$ to $\rho = -0.71$, which indicated that the equations predicted opposite trends. For τ_v a correlation of $\rho = 0$ was found. The experimental data of τ_v did not show significant results and the predictions indicated variations, which caused this low correlation. For $\varphi_{m,d}$, the opposite trend might have been present in the experimental results due to the phase lead introduced by the motion filter orders. In general, the equations for K_v, T_L and $\omega_{c,d}$ were found to be accurate predictors. For τ_v and $\varphi_{m,d}$, no conclusion on the prediction equations could be drawn, due to the absence of effects in the current experimental data and the experimental conditions themselves, respectively.

V.D. Human-Centered Simulator Benchmark

The experiment in this paper was performed in two flight simulators. More experiment replications in a broader environment consisting of more flight simulators, are necessary to strengthen the conclusions drawn. Consequently, a human-centered benchmark test is required, that has the purpose of identifying the effects of each simulator on the pilots that perform the experiment. The experiment in this paper indicated that relative trends between conditions are well reproducible across simulators, even in the presence of clear between-simulator biases in the results. A human-centered simulator comparison benchmark therefore might focus on at least two (motion) conditions, in order to investigate the relative effects between these conditions, instead of using one condition to find absolute differences. This may help overcome the pilot factors[29] of which experiment replications are subject.

VI. Conclusion

This paper describes the results of a tracking experiment performed to investigate the effects of different motion filter break frequencies ω_{mf} and motion filter orders O_{mf} on human control performance and behavior. Three motion filter orders and two motion filter break frequencies were tested in a factorial variation, in addition to two reference motion conditions: a full-motion and a no-motion condition. The experiment was performed on the VMS at NASA Ames Research Center and repeated on the SRS at Delft University of Technology in order to verify replication of the results. The motion system of the SRS was matched to the VMS using shaping filters. Head-down displays were used with the same graphics and the side stick was set to the same settings.

The effects of increasing the motion filter order O_{mf} on pilot behavior are equivalent to those of increasing the motion filter break frequency ω_{mf}, albeit less strong for the eight motion conditions considered in this experiment: pilots showed a similar decrease of performance and decrease in contribution of motion feedback on their control strategy. The results of this experiment indicate that pilots perform best with a low ω_{mf}. To prevent flight simulators from drifting, a low ω_{mf} could be compensated by a higher order filter (second or third order), without severely affecting pilot behavior.

The relative trends over the eight motion conditions were replicated well across the two simulators. However, even with meticulous attention paid to equalizing the simulator systems and the pilot population, the exact results between simulators for the same motion conditions were not replicated: biases were present within motion conditions between the two simulators. A future replication of experiments on multiple simulators, or even a human-centered benchmark test, might thus benefit from a focus on relative effects between a number of experimental motion conditions, instead of one setting in which the effects of the simulator are quantified.

References

[1]Boeing, *Commercial Market Outlook: 2018 - 2037*, Boeing Commercial Airplane Group, Seattle WA, USA, 2018, Retrieved from: https://www.boeing.com/commercial/market/commercial-market-outlook/.

[2]Airbus, *Global Market Forecast: 2018 - 2037*, Airbus S.A.S., Toulouse, France, 2018, Retrieved from: https://www.airbus.com/aircraft/market/global-market-forecast.html.

[3]Caird, J. K., "Persistent issues in the application of virtual environment systems to training," *Proceedings of the Third Annual Symposium on Human Interaction with Complex Systems*, Aug. 1996, pp. 124–132.

[4]Burki-Cohen, J. and Go, T., "The Effect of Simulator Motion Cues on Initial Training of Airline Pilots," *AIAA Modeling and Simulation Technologies Conference and Exhibit*, aug 2005.

[5]Burki-Cohen, J., Sparko, A., and Bellman, M., "Flight Simulator Motion Literature Pertinent to Airline-Pilot Recurrent Training and Evaluation," *AIAA Modeling and Simulation Technologies Conference*, aug 2011.

[6]Zaal, P. M. T. and Mobertz, X., "Effects of Motion Cues on the Training of Multi-Axis Manual Control Skills," *AIAA Modeling and Simulation Technologies Conference*, jun 2017.

[7]Zaal, P. M. T., Schroeder, J. A., and Chung, W. W., "Transfer of Training on the Vertical Motion Simulator," *Journal of Aircraft*, Vol. 52, No. 6, nov 2015, pp. 1971–1984.

[8]Federal Aviation Administration, "Stall Prevention and Recovery Training," Advisory Circular 120-109A, Nov. 2015.

[9]Zaal, P. M. T., Popovici, A., and Zavala, M. A., "Effects of False Tilt Cues on the Training of Manual Roll Control Skills," *AIAA Modeling and Simulation Technologies Conference*, jan 2015.

[10]Popovici, A., Zaal, P. M. T., and Pieters, M. A., "Time-Varying Manual Control Identification in a Stall Recovery Task under Different Simulator Motion Conditions," *AIAA Modeling and Simulation Technologies Conference*, jun 2018.

[11]Reid, L. D. and Nahon, M., "Flight Simulation Motion-Base Drive Algorithms: Part 1 - Developing and Testing the Equations," Tech. rep., UTIAS, 1985.

[12]Gouverneur, B., Mulder, J. A., van Paassen, M. M., Stroosma, O., and Field, E., "Optimisation of the SIMONA Research Simulator's Motion Filter Settings for Handling Qualities Experiments," *AIAA Modeling and Simulation Technologies Conference and Exhibit*, aug 2003.

[13]Pool, D. M., Damveld, H., van Paassen, M. M., and Mulder, M., "Tuning Models of Pilot Tracking Behavior for a Specific Simulator Motion Cueing Setting," *AIAA Modeling and Simulation Technologies Conference*, aug 2011.

[14]Pool, D. M., van Paassen, M. M., and Mulder, M., "Effects of Motion Filter Gain and Break Frequency Variations on Pilot Roll Tracking Behavior," *AIAA Modeling and Simulation Technologies Conference*, aug 2013.

[15]Pool, D. M., Zaal, P. M. T., Damveld, H., van Paassen, M. M., and Mulder, M., "Evaluating Simulator Motion Fidelity using In-Flight and Simulator Measurements of Roll Tracking Behavior," *AIAA Modeling and Simulation Technologies Conference*, aug 2012.

[16]Pool, D. M., Zaal, P. M. T., van Paassen, M. M., and Mulder, M., "Effects of Heave Washout Settings in Aircraft Pitch Disturbance Rejection," *Journal of Guidance, Control, and Dynamics*, Vol. 33, No. 1, 2010, pp. 29–41.

[17]Wieringen, A. T. V., Pool, D. M., van Paassen, M. M., and Mulder, M., "Effects of Heave Washout Filtering on Motion Fidelity and Pilot Control Behavior for a Large Commercial Airliner," *AIAA Modeling and Simulation Technologies Conference*, Aug. 2011.

[18]Steurs, M., Mulder, M., and van Paassen, M. M., "A Cybernetic Approach to Assess Flight Simulator Fidelity," *AIAA Modelling and Simulation Technologies Conference and Exhibit*, 2004.

[19]Bergeron, H. P., "Investigation of Motion Requirements in Compensatory Control Tasks," *IEEE Transactionson Man-Machine Systems*, Vol. MMS-11, No. 2, June 1970, pp. 123–125.

[20]van Gool, M. F. C., "Influence of Motion Washout Filters on Pilot Tracking Performance," *Piloted Aircraft Environment Simulation Techniques*, , No. AGARD-CP-249, 1978, pp. 19–1 – 19–5.

[21]Bray, R. S., "Visual and Motion Cueing in Helicopter Simulation," *TM-86818, NASA Ames Research Center*, 1985.

[22]Grant, P. R. and Reid, L. D., "Motion Washout Filter Tuning: Rules and Requirements," *Journal of Aircraft*, Vol. 34, No. 2, mar 1997, pp. 145–151.

[23]Hosman, R. J. A. W. and Advani, S. K., "Are Criteria for Motion Cueing and Time delays possible? Part 2," *AIAA Modeling and Simulation Technologies Conference*, aug 2013.

[24]Zaal, P. and Mobertz, X., "Effects of Motion Cues on the Training of Multi-Axis Manual Control Skills," *AIAA Modeling and Simulation Technologies Conference*, jun 2017.

[25]Schroeder, J. A., "Helicopter Flight Simulation Motion Platform Requirements," Tech. rep., NASA Ames Research Center, 1999.

[26]Grant, P. R., Yam, B., Hosman, R. J. A. W., and Schroeder, J. A., "The Effect of Simulator Motion on Pilot's Control Behavior for Helicoptor Yaw Tasks," *AIAA Modeling and Simulation Technologies Conference and Exhibit*, aug 2005.

[27]Ellerbroek, J., Stroosma, O., Wentink, M., Groen, E., and Smaili, H., "Effect of Sway and Yaw Motion on Perception and Control: A Multi-Simulator, Follow-Up Study," *AIAA Modeling and Simulation Technologies Conference and Exhibit*, aug 2006.

[28]Ellerbroek, J., Stroosma, O., Mulder, M., and van Paassen, M., "Identification of the Roles of Yaw and Sway Motion in Helicopter Yaw Control Tasks," *AIAA Modeling and Simulation Technologies Conference and Exhibit*, aug 2007.

[29]Ellerbroek, J., Stroosma, O., Mulder, M., and van Paassen, M. M., "Role Identification of Yaw and Sway Motion in Helicopter Yaw Control Tasks," *Journal of Aircraft*, Vol. 45, No. 4, jul 2008, pp. 1275–1289.

[30]Hodge, S., Perfect, P., Padfield, G., and White, M., "Optimising the yaw motion cues available from a short stroke hexapod motion platform," *The Aeronautical Journal*, Vol. 119, No. 1211, jan 2015, pp. 1–21.

[31]Hosman, R. J. A. W., Grant, P. R., and Schroeder, J. A., "Pre and Post Pilot Model Analysis Compared to Experimental Simulator Results." *AIAA Modeling and Simulation Technologies Conference and Exhibit*, aug 2005.

[32]Jex, H. R., Magdaleno, R. E., and Junker, A. M., "Roll tracking effects of G-vector tilt and various types of motion washout," *The 14th Annual Conference on Manual Control*, Nov. 1978, pp. 463–502.

[33]Jex, H. R., Jewell, W. F., Magdaleno, R. E., and Junker, A. M., "Effects of Various Lateral-Beam Washouts on Pilot Tracking and Opionio in the Lamar Simulator," Tech. rep., AFFDLTR-79-3134, 1979.

[34]Zaal, P. M. T. and Zavala, M. A., "Effects of Different Heave Motion Components on Pilot Pitch Control Behavior," *AIAA Modeling and Simulation Technologies Conference*, jun 2016.

[35]van Paassen, M. M. and Mulder, M., "Identification of Human Operator Control Behaviour in Multiple-Loop Tracking Tasks," *IFAC Proceedings Volumes*, Vol. 31, No. 26, sep 1998, pp. 455–460.

[36]Zaal, P. M. T., Pool, D. M., de Bruin, J., Mulder, M., and van Paassen, M. M., "Use of Pitch and Heave Motion Cues in a Pitch Control Task," *Journal of Guidance, Control, and Dynamics*, Vol. 32, No. 2, mar 2009, pp. 366–377.

[37]McRuer, D. and Jex, H., "A Review of Quasi-Linear Pilot Models," *IEEE Transactions on Human Factors in Electronics*, Vol. HFE-8, No. 3, sep 1967, pp. 231–249.

[38]Damveld, H. J., Abbink, D. A., Mulder, M., Mulder, M., van Paassen, M. M., van der Helm, F. C. T., and Hosman, R. J. A. W., "Measuring the Contribution of the Neuromuscular System During a Pitch Control Task," *AIAA Modeling and Simulation Technologies Conference*, aug 2009.

[39]Sinacori, J. B., "The Determination of Some Requirements for a Helicopter Research Simulation Facility," Tech. rep., NASA-CR-152066, Systems Technology Inc., 1977.

[40]Aponso, B. L., Beard, S. D., and Schroeder, J. A., "The NASA Ames Vertical Motion Simulator A Facility Engineered for Realism," *Royal Aeronautical Society Spring 2009 Flight Simulation Conference, London, UK*, June 2009.

[41]Pool, D. M., Mulder, M., van Paassen, M. M., and van der Vaart, J. C., "Effects of Peripheral Visual and Physical Motion Cues in Roll-Axis Tracking Tasks," *Journal of Guidance, Control, and Dynamics*, Vol. 31, No. 6, nov 2008, pp. 1608–1622.

[42]Zaal, P. M. T., Schroeder, J. A., and Chung, W. W., "Transfer of Training on the Vertical Motion Simulator," *Journal of Aircraft*, Vol. 52, No. 6, nov 2015, pp. 1971–1984.

[43]Schroeder, J. A. and Grant, P. R., "Pilot Behavioral Observations in Motion Flight Simulation," *AIAA Modeling and Simulation Technologies Conference*, aug 2010.

[44]ICAO, "Document 9625, Volume 1, Attachement F: Frequency-Domain Motion Cueing System Performance Test," Tech. rep., ICAO, 2009, ISBN 978-92-9231-341-8, obtained online.

[45]Danek, G. L., "Vertical Motion Simulator Familiarization Guide," Tech. rep., NASA-TM-103923, 1993.

[46]Lehmer, R. and Chung, W., "Image Dynamic Measurement System (IDMS-2) for flight simulation fidelity verification," *AIAA Modeling and Simulation Technologies Conference and Exhibit*, aug 1999.

[47]Stroosma, O., van Paassen, M. M., Mulder, M., and Postema, F., "Measuring Time Delays in Simulator Displays," *AIAA Modeling and Simulation Technologies Conference and Exhibit*, aug 2007.

[48]Sawilowsky, S. S., "Nonparametric Tests of Interaction in Experimental Design," *Review of Educational Research*, Vol. 60, No. 1, mar 1990, pp. 91–126.

[49]Field, A., *Discovering Statistics Using SPSS (Introducing Statistical Methods series)*, Sage Publications Ltd, 2005.

[50]Scheirer, C. J., Ray, W. S., and Hare, N., "The Analysis of Ranked Data Derived from Completely Randomized Factorial Designs," *Biometrics*, Vol. 32, No. 2, jun 1976, pp. 429.

[51]Sokal, R. R. and Rohlf, F. J., *Biometry: The Principles and Practices of Statistics in Biological Research*, W. H. Freeman, 1994.

[52]Zaal, P. M. T., Pool, D. M., Chu, Q. P., Mulder, M., van Paassen, M. M., and Mulder, J. A., "Modeling Human Multimodal Perception and Control Using Genetic Maximum Likelihood Estimation," *Journal of Guidance, Control, and Dynamics*, Vol. 32, No. 4, jul 2009, pp. 1089–1099.

[53]Valente Pais, A. R., Pool, D. M., De Vroome, A. M., van Paassen, M. M., and Mulder, M., "Pitch Motion Perception Thresholds During Passive and Active Tasks," *Journal of Guidance, Control, and Dynamics*, Vol. 35, No. 3, may 2012, pp. 904–918.

[54]Nieuwenhuizen, F. M., Mulder, M., van Paassen, M. M., and Bülthoff, H. H., "Influences of Simulator Motion System Characteristics on Pilot Control Behavior," *Journal of Guidance, Control, and Dynamics*, Vol. 36, No. 3, may 2013, pp. 667–676.

[55]Toothaker, L. E. and Horng Shing Chang, "On "The Analysis of Ranked Data Derived from Completely Randomized Factorial Designs"," *Journal of Educational Statistics*, Vol. 5, No. 2, 1980, pp. 169.